2005

Two-dimensional scour hole problem: Role of fluid structures

Alex Bey
University of Windsor

TWO-DIMENSIONAL SCOUR HOLE PROBLEM: ROLE OF FLUID STRUCTURES

by

Alex Bey

A Thesis

Submitted to the Faculty of Graduate Studies and Research

through the Department of Civil and Environmental Engineering

in Partial Fulfillment of the Requirements for

the Degree of Master of Applied Science at the

University of Windsor

Windsor, Ontario, Canada

Your file Votre référence
ISBN: 0-494-09747-7
Our file Notre référence
ISBN: 0-494-09747-7

ABSTRACT

An experimental program was carried out to further understand the scour caused by a plane wall jet. To this end, a two-dimensional laser Doppler anemometer was used to characterize the velocity field at various stations in the scour hole region. Present observations indicate that different types of flow structures influence scour at different time periods. Following vigorous digging caused principally by jet shear forces and impingement at the start of the test, the flow was characterized by the presence of longitudinal axial vortices, turbulent bursts and movement of the jet impingement point during the later stages. Attempts have been made to identify the role of these structures at near asymptotic conditions. The scour hole region was characterized by the presence of randomly forming and disappearing streaks, longitudinally located concave shaped depressions, rolling and ejection of sand grains. Through analysis of higher order moments and quadrant decomposition, sweep and ejection type events were observed. Such events contribute to scour and need to be incorporated in future modeling work.

DEDICATION

This thesis is dedicated in memory of my father, Mr. Michael Bey,

ACKNOWLEDGEMENTS

I thank God for granting me life.

My profound appreciation, gratitude and most heart felt thanks to my advisor Dr. Ram Balachandar for his time, invaluable guidance, advice, inspiration, thoughtful insights, encouragement and support throughout my research on this thesis.

My sincere thanks to my committee members; Dr. R. Barron and Dr. R. Carriveau for their advice, encouragement and for their time. To Mr. Richard Clark, Mr. Lucian Pop and Mr. Patrick Seguin, thank you for all your assistance during my work. Your prompt action and devotion to remedy the problems that came up during the setup and testing program assisted the timely completion of my study.

Mr. M.A.A. Faruque, thank you for your assistance during my test runs.

This list could be endless, to all that I cannot mention here, and my colleagues who helped make this a success, a big thank you.

Financial support from the University of Windsor, and the Natural Sciences and Engineering Research Council of Canada is also greatly appreciated.

TABLE OF CONTENTS

LIST OF TABLES

LIST OF FIGURES

NOMENCLATURE

ACRONYMS

2-D = Two-dimensional

CFD = Computational Fluid Dynamics

LDA = Laser Doppler Anemometer

rms = root-mean-square

ENGLISH SYMBOLS

B = width of the flume

b_o = width of jet (nozzle size)

d_N = bed material diameter, N% of which is finer by weight (N = 5, 10, 16, 30, 60,84, 95)

$D_u = \overline{uv^2}$

$D_v = \overline{u^2 v}$

g = gravitational acceleration

h = maximum height of ridge

H = tailwater depth

t = time

u = instantaneous mean velocity in the streamwise direction

$\overline{uv}$ = turbulent shear stress

$\overline{uv^2}$ = turbulent diffusion in the x-direction

$\overline{u^2}$ = streamwise turbulent intensity

$\overline{u^2 v}$ = turbulent diffusion in the y-direction

$\overline{u^3}$ = streamwise flux of the turbulent kinetic energy $\overline{u^2}$

$\bar{U}$ = mean velocity at any point in streamwise direction

U_o = average jet velocity

U_{max} = maximum streamwise velocity at any station

$\overline{v^2}$ = turbulent intensity normal to the initial bed

$\overline{v^3}$ = flux of turbulent kinetic energy $\overline{v^2}$ normal to the initial bed

v = instantaneous mean velocity normal to the sand bed

$\overline{V}$ = mean velocity normal to the sand bed

x = longitudinal distance from the nozzle

x_c = distance of maximum scour depth from the nozzle

x_m = axial distance from the gate

$y_{½}$ = jet half width

y = lateral distance from the nozzle

y_t = depth of water above the bed

z = lateral distance from the nozzle

GREEK SYMBOLS

$\Delta\rho$ = difference between mass densities of water and bed material

ε_m = maximum scour depth

ν = kinematic viscosity

ρ = mass density of water

σ_g = geometric standard deviation of bed material = $(d_{84}/d_{16})^{0.5}$

DIMENSIONLESS COMBINATIONS

C_z = Coefficient of curvature = $d^2_{30}/(d_{60}d_{10})$

$F_o = U_o \Big/ \sqrt{g(\Delta\rho/\rho)d_{50}}$

$F_r = U_o \Big/ \sqrt{gb_o}$

$Re_j = U_o b_o/\nu$

CHAPTER 1

INTRODUCTION

Scour is the removal of sediment due to moving water over an erodible surface. It is usually more significant during high flows, when moving water has more energy (turbulence and velocity) to lift and transport the sediment. Scour prediction and control have been considered very important in hydraulic engineering practice, as sediment removal can cause significant local scour and possible damage to engineering works. According to Mason and Arumugam (1985) plunging water flow could weaken engineered structures. Kouchakzadeh and Townsend (1997) point out that a very large percentage of bridge failures can be attributed to pier and abutment scour. Engineers have resorted to laboratory studies of the interaction of plane wall jets with non-cohesive sand beds, and other forms of two-dimensional jet scour to understand the mechanisms of scour. Hogg et al. (1997) pointed out that a comprehensive understanding of the scour mechanism remains elusive because of the complex nature of the flow field. The hydrodynamic characteristics of the jet flow and the concave shape of the eroded bed further increases the complexity. Despite these assertions, Rajaratnam and co-researchers have made significant contributions in this area (e.g. Rajaratnam and Berry, 1977, Belatos and Rajaratnam, 1977, Rajaratnam and Macdougall, 1983, Wu and Rajaratnam, 1995, Rajaratnam et al., 1995). Other related studies include that of Laursen (1952), Ali and Lim (1986), Johnston (1990), Breusers and Raudkivi (1991), Mohamed and McCorquodale (1992), Chatterjee et al. (1994), Balachandar and Kells (1997), Kells et al. (2001) and Dey and Barbhuiya (2004).

The total elimination of scour is possible, but for practical reasons and economic considerations this cannot be easily attained, therefore methods are sought to control the process and thereby minimize the risk of failure.

1.1 General Remarks

The relevant terminologies in this thesis are defined below:

1.1.1 Scour

i. *Local scour* is the morphodynamic change caused by an altered flow pattern around an object located on the bed resulting in the formation of a scour hole.

ii. *Clear water scour* occurs when the bed material is not in motion. The net sediment transported is essentially zero. Clear water scour occurs when the shear stress induced by the water flow exceeds the critical shear stress of the bed material.

1.1.2 Submergence

Submergence is a dimensionless quantity, defined as the ratio of the depth of water above the bed (y_t) to the width of the jet opening (b_o) (c.f. Figure 4.2.1). Submergence can be said to be high or low, though there is no established delineation of high or low submergence. Researchers have based this description on their individual observations. However, Ali and Lim (1986) have suggested that the effect of tailwater on scour hole development becomes insignificant for $y_t/b_o > 16$. However, recent studies (Faruque (2004), Sarathi (2005)) have shown that this value can be as low as six.

1.1.3 Turbulent flow

Turbulent flow or turbulence is a flow regime that is characterized by randomly fluctuating local velocities and pressures in space and time. The dimensionless Reynolds number identifies flow conditions that lead to turbulent or laminar flow. Turbulence occurs naturally, examples include river flow, cloud movement and combustion in automobile engines, just to mention a few. High Reynolds number flows are considered to be turbulent. Studies explicitly relating turbulence to scour is rare and is an aspect that needs attention.

1.1.4 Jet classification

Jets are defined as the emission of fluid into a surrounding fluid of zero or lower relative velocity. Depending on the density of the surrounding fluid, the jet can be classified into two types:

i) Non-buoyant : Jet and surrounding fluid have the same density.

ii) Buoyant : Jet density is less than that of the surrounding fluid .

Jets are classified into four categories based on their geometric configuration. These are:

i) Free jet : A jet flow that is not influenced by boundaries, or the boundaries are relatively far from the jet location.

ii) Wall jet : A jet flow that is set parallel to the undisturbed bed level such that it flows tangentially to it.

iii) Offset jet : A jet flow that is set some distance away from the bed.

iv) Impinging jet : A jet that impinges at an angle onto the undisturbed bed level or boundary.

Jets, based on their aspect ratios, can further be described as two-dimensional or three-dimensional. They are said to be submerged when they exit into a fluid of equal or higher density, otherwise, they are referred to as unsubmerged. Lastly, depending on the flow type, they can be said to be laminar or turbulent jets. This study is on clear water local scour of non-cohesive soils by non-buoyant turbulent plane wall jets under submerged conditions. Practical examples of this type of flow include flows under sluice gates or submerged hydraulic jumps in rectangular channels.

1.2 Summary

In general, many empirical relationships have been suggested to describe some aspects of the scour process and attempts to theoretically model the process have been semi-empirical at best. Progress in numerically modeling the flow, though slow, is evolving as new techniques are coming to the forefront. In a recent study, Hopfinger et al. (2004) attempted to qualitatively explain the scour process and identify the work of turbulent structures. In the keynote address at the 2nd International Conference on Scour and Erosion held in Singapore, Annandale (2004) stressed the need to understand the role of turbulent fluctuations in future scour analysis.

The present study focuses on the velocity field in the scoured region created by a plane turbulent wall jet flowing over a cohesionless sand bed boundary submerged in water and attempts to further understand the role of turbulent fluid structures that influence scour. Besides the mean flow, the higher-order velocity moments will be

evaluated and a quadrant decomposition carried out to understand the role of turbulent events.

1.3 Objectives and Scope

1.3.1 Objectives

Based on the summary, the objectives of this study are:

(1) To further understand scour caused by a plane wall jet.

(2) Identify the fluid structures influencing scour.

(3) Examine and characterize these fluid structures in the scour region at asymptotic conditions.

1.3.2 Scope

The remaining sections of this thesis are laid out in the following manner. Relevant literature dealing with scour caused by wall jets is reviewed in Chapter 2. Chapter 3 describes the experimental details including the setup and the procedures adopted. The data and results obtained therein are presented and discussed in Chapter 4. The conclusions from the present research and recommendations for future research work are presented in Chapter 5.

CHAPTER 2

LITERATURE REVIEW

2.1 Introduction

The localized scour phenomenon has been a subject of extensive investigations by many researchers. Thus numerous literature abounds for scour caused by turbulent jets with different geometrical configurations and tailwater depths. A review dating from the pioneering investigation of scour due to a jet by Rouse (1939) can be found in Karim and Ali (2001). Numerous studies have been conducted with plane wall jets interacting with cohesionless sand beds. A common feature noted by the various researchers is the initial rapid development of the scour hole which eventually attains a state where the scour profile does not change significantly with time. Furthermore, other studies have noted the presence of various flow regimes depending primarily on tailwater depth. As a result of these studies, many empirical relationships have been suggested to describe some aspects of the scour process and attempts to theoretically modeling the process have been semi-empirical at best.

2.2 Scour by Plane Turbulent Wall Jets

A turbulent jet issuing from any slot over a flat cohesionless sand bed almost instantaneously dislodges the sand grains due to its scouring potential as a result of the high incoming velocity. The dislodged sand grains are lifted and held in suspension and rapidly transported downstream. The entrainment, transportation and subsequent deposition of sand grains is also influenced by the properties of the sand grains.

2.2.1 Experimental prediction of scour

Laursen (1952) observed that at the start of jet action, sand grains were eroded rapidly from the bed as bed load, forming a scour hole and a mound downstream. The vertical dimensions of the scour profile increase rapidly. He observed that a greater portion of these eroded sand grains were deposited on the upstream face of the mound. Some of these sand grains fell back into the scour hole when the natural angle of repose was attained. Others were entrained by the flow and lifted into suspension by the upward currents of the flow. Large counterclockwise eddies were also noticed and these returned suspended sand grains into the scour hole.

Laursen (1952) proposed that the scour profile development varied logarithmically with time. This was valid within some time range beyond which the scour geometry reached an end state. This end state is referred to as asymptotic, ultimate or equilibrium state of scour. He further explained that the enlargement of the flow section would result in reduction of velocity along the boundary and therefore a reduction in capacity for transport of sand grains. The rate of scour must then decrease and after some duration, an asymptotic state could be achieved. He suggested that there must be some boundary position at which the velocity decreases to a value incapable of sand grain transport and rate of scour becomes zero or negligible.

In similar experiments conducted by Tarapore (1956) he summarized the flow as an initial turbulent state where the length of the scour hole is random. This is followed by the transportation of bed material, and finally the reduction in velocities at the boundaries of the hole leading to the asymptotic state. He suggested that the time taken

to reach the asymptotic state and the geometry of the scour hole were functions of the sand grain properties, the width of the jet opening, the jet velocity and tailwater depth.

Whilst conducting experiments with sand and polystyrene particles, Rajaratnam (1981) also found that the profile of the eroded bed varied with time till the asymptotic state was reached. He established that the development of the scour profile was related to the densimetric particle Froude number, defined as $F_o = U_o / \sqrt{g(\Delta\rho/\rho)d_{50}}$.

Rajaratnam and Macdougall (1983) noted that at the asymptotic scour state, the maximum scour hole depth (ε_m) and the corresponding axial distance from the gate (x_m) were related to the magnitude of the densimetric Froude number. They however noted that the magnitude of the ratio ε_m/b_o is relatively less for the corresponding case at relatively deeper tailwater, for any densimetric Froude number. They also noted that the maximum scour location is pushed farther downstream, however the characteristic scour mound which forms at the downstream end of the scour hole at high submergence was absent when the tailwater depth was equal to the jet thickness (b_o). Further to the above, they also noted that the eroded bed profiles in the asymptotic state were approximately similar.

Johnston (1990) conducted experiments with an offset jet using four values of submergences between 0.52 - 4.03. He noted that the development of the scour hole depended on the location of the boundary of the attachment jet. He explained his findings that at the submergence of 4.03, the jet mainstream was attached to the bed and rapidly developed a scour hole with the mound positioned downstream of the hole. He termed this phenomenon as 'bed jet' scour hole regime. At a submergence of 0.52, he noted that the jet was directed to the free surface, developing a longer but shallow scour

hole in the streamwise direction. The mound was also less obvious and tended to move downstream fairly quickly. He described this scour hole mechanism as the 'surface jet' regime. For the intermediate submergence ranges, he noted that at one instant, the jet was attached to the bed, developing what he had earlier described as a 'bed jet' scour hole regime. Then suddenly, the mound slumps back into the scour hole partially filling it. He noted that this cyclic pattern of scouring and re-filling occurred throughout the test.

In their study of deeply submerged offset turbulent jets, Ali and Neyshaboury (1991) also confirmed that scour geometry was a function of particle size and the densimetric Froude number. However, they observed that for the same jet opening, an offset jet created a deeper asymptotic scour depth as compared with non-offset jets.

In dealing with submerged plane wall jets issuing below a sluice gate, Balachandar and Kells (1997) noted the presence of two flow regimes comprised of a digging phase as a result of a bed jet and a subsequent refilling phase due to the formation of a surface jet. The digging process usually occurred for relatively short periods of time (10 - 25 s) as against the refilling phases that lasted between 100 - 1000 s. The two flow regimes were found to alternate. The downstream movement of the bed material was accompanied by the rapid digging of a hole in the sand bed near the sluice gate. The digging process was immediately followed by a gradual upstream transport of the sand grains and a refilling of the scour hole. They concluded that the maximum depth of scour observed during the short-duration digging was greater than was observed during any other phase of the scour process.

Aderibigbe and Rajaratnam (1998) studied erosion by plane turbulent wall jets with varying submergences. They observed that when the Froude number $F_o > 5$ the jet

oscillated between a position along the bed and a position in the horizontal direction with a period of 5 -10 s. They also noted that there was significant scour and subsequent transportation of this eroded material when the jet was directed towards the bed. A reverse flow was also observed, which transported the sand grains that collapsed from the scour mound into the mid-section of the scour hole.

Balachandar et al. (2000) conducted tests in the submergence range of 4.0 - 8.9 and also observed this unstable jet phenomenon as reported by Johnston (1990). They reported the occurrence of two cyclically alternating flow fields and the presence of a mound which formed just downstream of the scour hole. In one cycle, the plunging of the jet towards the bed and an associated digging of the sand bed was predominant. In another instance, the jet flips to the surface and forms what was referred to as a 'surface jet'. This resulted in a partial refilling of the scour hole. They also reported that this pattern repeated itself throughout the test.

2.2.2 Numerical prediction of scour

Ushijima (1996) developed a numerical prediction for local scour on a sand bed due to turbulent flows. He based his method on the Lagrangian-Eulerian formulation, where three-dimensional body-fitted coordinates are generated to represent the sand bed profile being unsteadily deformed by the flow. The equations for momentum, turbulent quantities, and sand concentration were discretized in a Lagrangian scheme so as to preserve second-order accuracy with respect to time and space. Using the continuity equation, he predicted sand bed profiles by evaluating the total flux consisting of the bed and suspended loads as a result of the tractive and convective forces of the turbulent

flow. The results from the numerical method compared favourably with the results obtained from a local scour experiment.

Karim and Ali (2001) have described a testing procedure for investigating the suitability of the FLUENT CFD package in simulating flow patterns, generated by a turbulent water jet impinging on rigid horizontal and scoured beds. The scoured beds were predicted at various times of the scouring process. The numerical scheme provided by FLUENT was used to predict the 2-D flow velocity distribution and the bed shear stress for both flat bed and scoured bed. The computational results showed a close agreement with the various selected experimental results.

In their numerical simulation of scour by a plane wall jet, Neyshabouri et al. (2001) presented the time rate deposition or scour at the bed by solving the continuity equation for sand grain. They noted that the flow pattern and the shear stress at the bed, which primarily influences the scour process, can be predicted correctly by the hydrodynamic component of the model.

Whilst conducting studies with a two-dimensional turbulent wall jet over a non-cohesive sand bed, Hogg et al (1997) demonstrated that turbulent wall jets flowing over rough boundaries could not be simply approximated by free jet scaling. Thus, they modified the results for flows over fixed boundaries to study those over erodible boundaries. They further utilized simple mobilizing and resisting moments on the particles at the surface of the sloping bed to obtain critical conditions for incipient particle motion. This enabled the prediction of the characteristic dimensions of the steady-state scour hole. They also formulated a model of the progressive erosion of the scour hole by using a bed-load model of the rate of particle transport. This was achieved

by employing an expression for sand grain volume. Though this model had some inherent assumptions, it agreed favorably well with experimental results.

2.2.3 Turbulent structures and scour

In a recent study, Hopfinger et al. (2004) conducted tests in the submergence range of 2.75-8.8. For the case of the submergence of 4.4 and 8.8, they reported a quasi-steady state of scouring. They observed loose sediment streaks or longitudinal ridges on the upstream-facing sediment slope scour hole and referred to these as signatures of intense longitudinal vortices that lift up sediment. They explained that the origin of these vortices were due to Görtler instability and showed that the concave shaped scour hole and other flow conditions favored such instability of the boundary region of the turbulent wall. They further suggested that sediment transport and the consequent scouring mechanism was due to turbulence created by Görtler vortices. In their conclusion, they proposed that scouring and the subsequent sediment transport is primarily due to the instability of the turbulent wall layer due to the concave curvature of the water sediment interface in the turbulent wall region and further proposed new scaling laws relating time and the attainment of the quasi-steady scour depth.

2.3 Evaluation of Literature Review

The literature review has discussed the experimental and numerical studies that have contributed to the understanding of scour mechanism. Some previous studies have utilized numerical and semi-empirical models to explain the scour phenomenon, but at best, these have had to include various assumptions to favorably compare with experimental data. On evaluation, there are indications that though the agents responsible for scouring have been broadly identified, relatively little research has been conducted into the qualitative understanding of the mechanism of scour caused by plane wall jets. This area needs to be further explored, taking into consideration the current state-of-the-art measuring techniques and technologies that are available. The roles of fluid structures and associated turbulence within the scour region need to be examined and clarified. It is therefore in order that a qualitative analysis of the flow field is carried out to identify the fluid structures and their roles in causing scour.

On the basis of the current literature review, the specific objectives of the study include:

1. Conducting experiments at high submergence.
2. Identify the fluid structures influencing scour.
3. Examine and characterize these fluid structures in the scour region at asymptotic conditions.

CHAPTER 3

EXPERIMENTAL SETUP AND PROCEDURE

3.1 Experimental Setup

A schematic drawing of the open channel flume and experimental setup is shown in Figure 3.1. Figure 3.2 shows the nozzle opening in the front view and Figure 3.3 shows the transparent acrylic wall and sand bed in the side view. The experiments were performed in a recirculating open channel flume. The main component of the flume is a rectangular channel 15 m long, 0.4 m wide and 0.9 m deep. The walls are made of transparent acrylic to allow visual observations and the passage of laser light. A piping arrangement discharges water into a settling chamber, which then exits through flow straightners through the nozzle, on to the sand bed. The nozzle width is 0.4 m with an opening b_o = 25 mm. The nozzle opening is set flush with the horizontal sand bed which is 0.3 m deep, 0.4 m wide and 2.5 m long. The median sand grain diameter, d_{50}, is 2.15 mm with a geometric standard deviation σ_g of 1.28. The initial sand bed was not compacted and fully saturated prior to the start of tests. The jet was operated to permit only local scour and there was no net transport of sand beyond the edge of the sand bed. The downstream end of the flume was provided with a sand trap to prevent any accidental transport of sand into the flow system.

3.2 Laser Doppler Anemometry

The Laser Doppler Anemometer, or LDA, is a widely accepted tool for fluid dynamic investigations in gases and liquids and has been used as such for more than three decades. It is a well-established technique that gives information about flow velocity. The LDA's non-intrusive principle and directional sensitivity make it very suitable for

applications with reversing flow and where physical sensors are difficult or impossible to use. The particular advantages of the method are the non-intrusive measurement, high spatial and temporal resolution and the need for no calibration. The use of the LDA however requires tracer particles in the flow. The system primarily consists of a laser source, an optical arrangement and a Bragg cell. A photo-detector converts the fluctuating light intensity to electrical signals. The LDA system used in this experiment is powered by 300-mW argon-ion laser. The LDA system was operated in backward scatter mode. In this experiment, the probe volume, that is the spatial domain arising from the intersection of the exit beams from the optical fibres focused by the probe lens was $0.124 \times 0.123 \times 1.65$ mm^3. The flow had sufficient naturally occurring particles and therefore no artificial seeding was required. Due to the restrictions imposed by the geometry of the transmitting optics and the channel support structures, measurements were not possible at locations closer than a distance of $2b_o$ ($\approx$50 mm) downstream of the nozzle exit. The fiber optic probe was mounted on a two-dimensional stepper motor driven traversing mechanism capable of repeatedly attaining the same location with an accuracy of $\pm$0.01 mm. Measurements were conducted along the centreline of the channel and at other off-set locations at various distances from the nozzle.

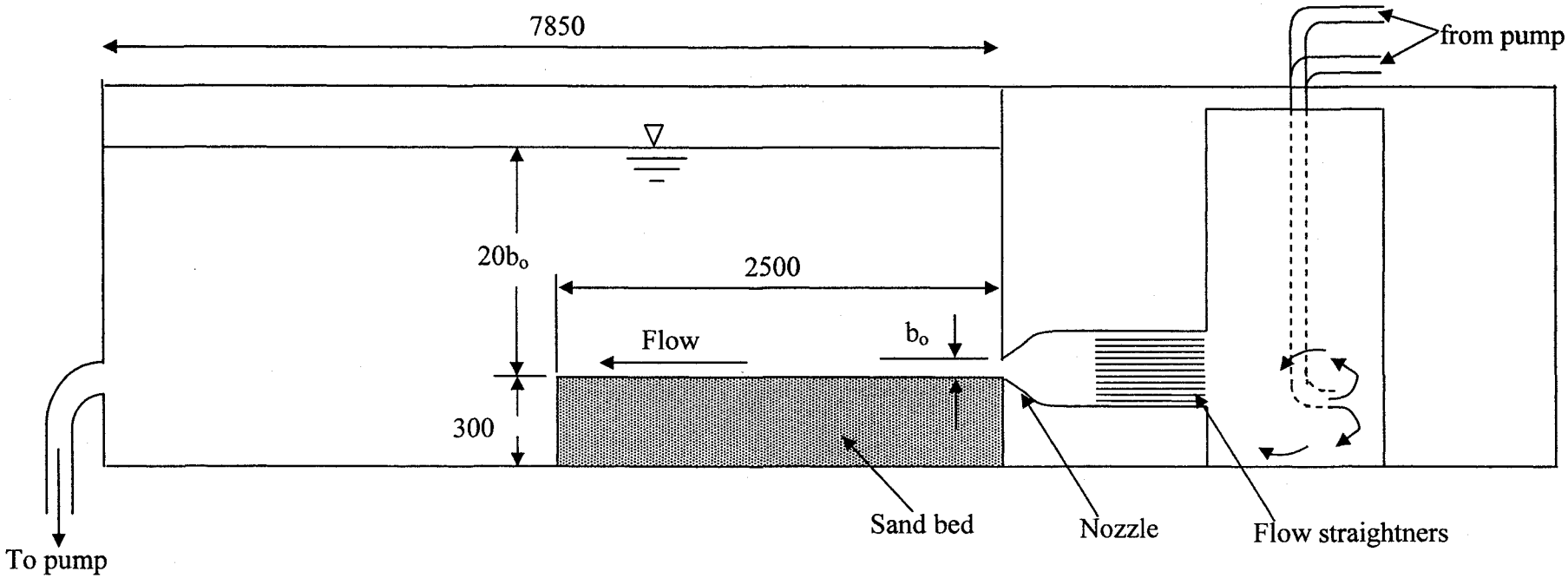

(All dimensions are in mm, not drawn to scale)

Figure 3.1: Experimental setup

Fig 3.2: Front view of the flume and nozzle exit

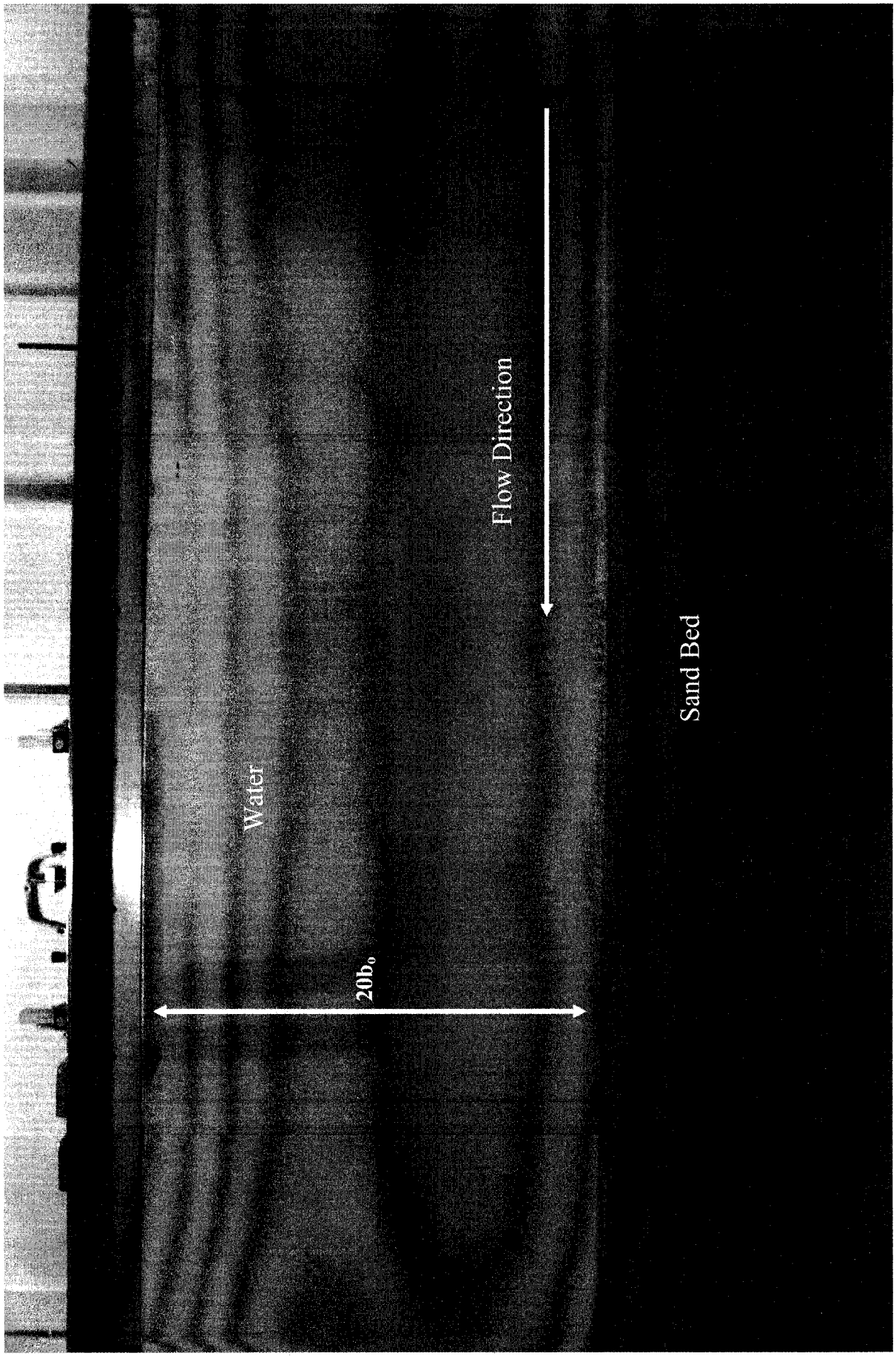

Fig 3.3: Side view transparent glass wall and sand bed

3.3 Test conditions

A summary of the tests is presented in Table 3.1. The tailwater depth (H), was held constant at $20b_o$. The jet exit velocity (U_o) for the tests was held constant at 1.0 m/s and 1.27 m/s, respectively. These correspond to jet exit Reynolds numbers ($Re_j = U_o b_o/\nu$) of 25,000 and 32,000 and flow Froude numbers at the nozzle exit $F_r = U_o/\sqrt{gb_o}$ of 2 and 2.54, respectively. The corresponding densimetric Froude numbers, $F_o = U_o/\sqrt{g(\Delta\rho/\rho)d_{50}}$, are 5.4 and 6.8, respectively. It should be noted that the pumping arrangement yielded the maximum jet exit velocity of 1.27 m/s and test velocities below 1.0 m/s were not sufficiently turbulent. The test at U_o = 1.0 m/s (Test A) was repeated thrice, mainly to ensure repeatability and also to obtain further validation of flow features that were noticed. The values of Re_j and F_o were chosen to be in the range of that used in previous studies.

TEST	U_o (m/s)	F_r	F_o	Tailwater	Duration(days)
A	1.00	2.00	5.40	**$20b_o$**	18
B	1.27	2.50	6.80	**$20b_o$**	12
C	1.00	2.00	5.40	**$20b_o$**	14
D	1.00	2.00	5.40	**$20b_o$**	8

Table 3.1: Summary of test conditions

3.4 Test Procedure

The sand bed was initially leveled to zero slope and the flume filled with water to a depth of $20b_o$. The flow was started and the desired velocity was set by adjusting the pump valves downstream. Thereafter, the water was drained. The sand bed leveled to zero slope as before and the flume filled to a depth of $20b_o$ (Figure 3.1). The tests were conducted uninterrupted over a period of 8 ~ 12 days. For each test, the uniformity of the velocity distribution across the nozzle exit was verified. Further, constancy in test conditions was ensured by monitoring the velocity at the nozzle axis for the entire test duration (8 ~ 12 days). Video images are taken at the start of the experiment and at various time intervals. Each test was run, until near asymptotic conditions are attained (≈72 hrs) and velocity profiles were obtained along the flume axis at various axial stations covering a range $2 \leq x/b_o \leq 50$. The scour profiles were obtained using a digital point gauge with a resolution of ±0.01 mm mounted on a traversing system along the length of the flume. The geometric profiles of interest include the centreline scour profile, measured at 75 mm centres, across the width of the flume and the cross-section in the mound region.

The scour hole shape as a function of time, sand grain movement in the scour hole and its variation across the width of the channel was studied with a video imaging system. Dye injection was used to enhance flow visualization. In this study $(\overline{U})$ and $(\overline{V})$ denote the mean velocity in the x and y direction respectively. u and v denote the fluctuations about the mean whilst u' and v' denote the root-mean-square (rms) values. The other variables of interest also include triple-correlations ($\overline{uv^2}$, $\overline{u^2v}$, $\overline{u^3}$, $\overline{v^3}$) and quadrant decomposition of the velocity measurements.

3.5 Uncertainty Estimates

The statistical uncertainties, at the 95% confidence level, are presented for the mean velocities and turbulence fluctuations. A more complete uncertainty analysis is presented in Appendix C.

CHAPTER 4

RESULTS

4.1 Introduction

The present tests can be classified to be under the high submergence flow regime ($H/b_o = 20$). It is worth noting that no alternate jet flicking towards the free surface and bed is observed as is characteristic of flows at low submergence (Balachandar et. al. 2000). The following general description based on visual observation applies to the scour process for both tests A and B. As the jet exits the nozzle and interacts with the sand bed, scour progresses rapidly in the longitudinal direction. In the initial stages of scouring, some of the bed material goes into suspension and is rapidly transported and deposited downstream as a mound. With progress in time, the scour hole depth increases and after a relatively long duration, attains equilibrium state. Turbulent bursts can be seen occurring in the vicinity of the maximum scour depth, contributing to the transport of the sand particles. The turbulent bursts do not cause large scale scouring action. These turbulent bursts are relatively weak and therefore unable to cause large scale suspension of the particles and only cause rolling and sideways movement of the sand particles. These bursts occur quite frequently, though with increase in time, they appear to reduce. However, these bursts persisted throughout the test period.

4.2 Visual Observations

The following detailed visual observations were made with the aid of dye injection and observing the movement of sand particles at various locations in the flow

field. Sectional and plan view of the scour region with the definition of variables is shown in Figure 4.2.1. Based on a detailed review of the video tapes and observations made during repeated experiments, the following five time zones are chosen to describe the flow.

4.2.1 $t \leq 600$ s: (Time zone A)

When the plane wall jet exits the nozzle, the flow is initially parallel to the sand bed and following a very short duration, scour commences. Scour is very vigorous and a hole is formed downstream of the nozzle. Sand is deposited as a mound downstream of the scour hole. The longitudinal scour profile is fairly two-dimensional and constant across the width of the flume. As the scour hole progresses in the longitudinal direction, the jet impingement on the downstream slope of the hole causes a large scale suspension of bed material into the flow. An example of this suspension at early stages of the scouring process is shown in Figure 4.2.1.1. Figure 4.2.1.2 shows an instantaneous video image indicating sand grains suspended all the way to the free surface (~ 20 b_o). The particles are predominantly transported in the downstream direction though some fall back into the hole. This type of scouring action has been reported by all related previous studies.

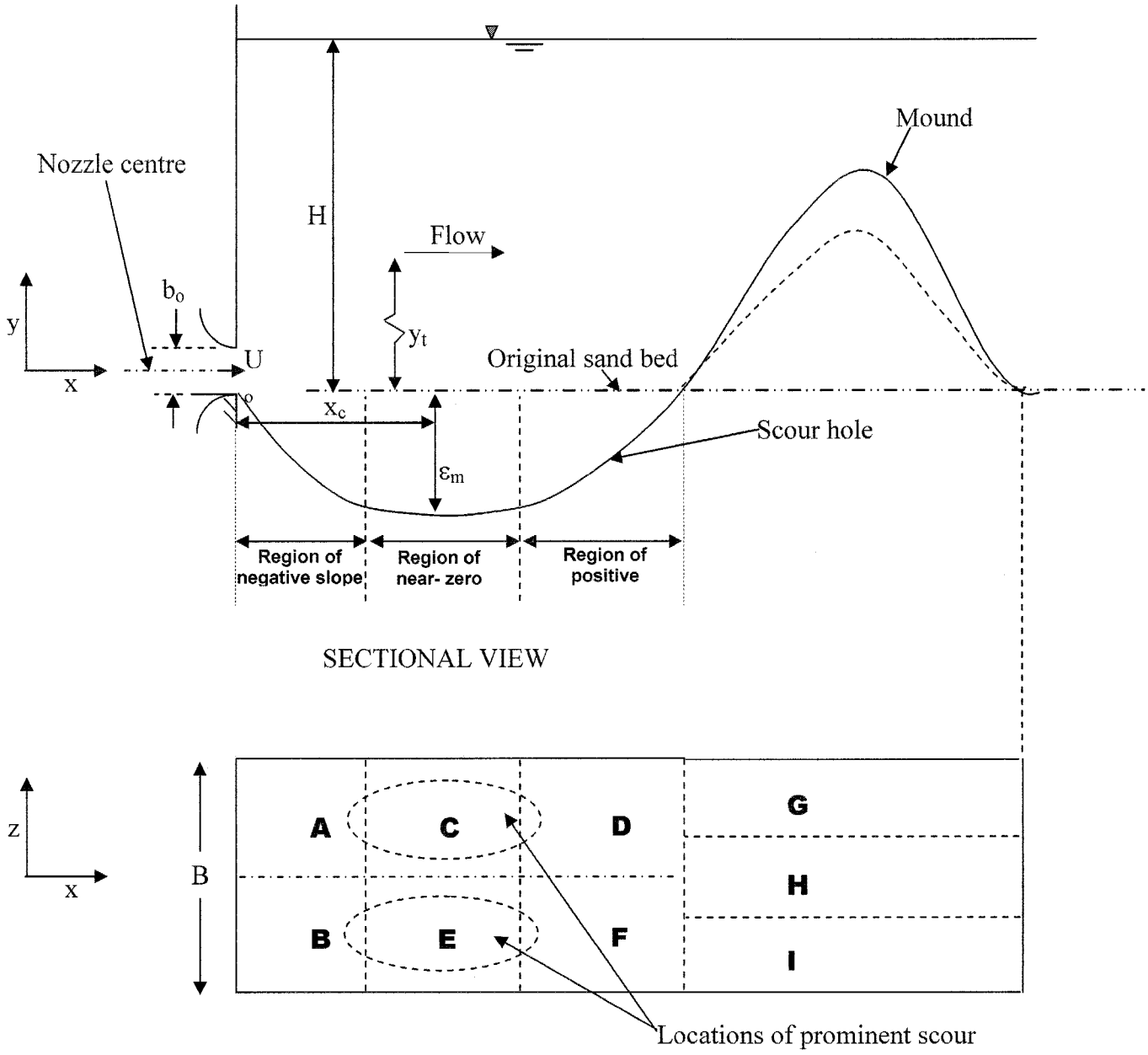

Figure 4.2.1: Definition sketch

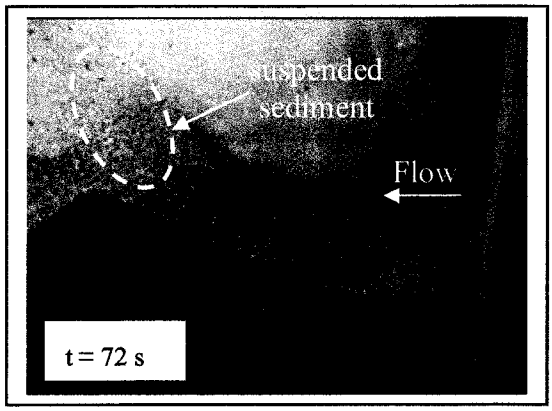

Figure 4.2.1.1: Sand grain suspension at t = 72 s

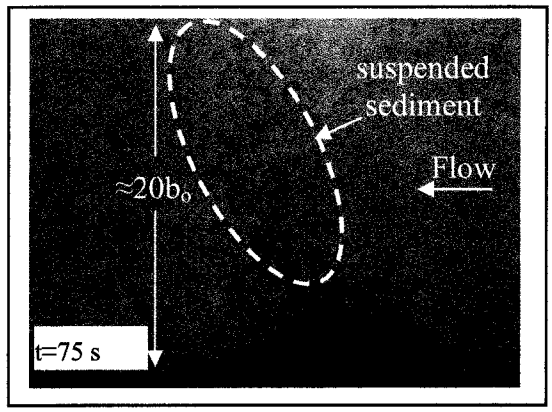

Figure 4.2.1.2: Sand grain suspension all the way to the surface at t = 75 s

4.2.2 600 s ≤ t ≤ 3 hrs: (Time zone B)

With progress in time (t > 600 s), the jet expands into a larger space (due to the presence of a larger and deeper scour hole). The jet is confined by the bed on one side and can be considered to be relatively free on the other side. The large scale suspension of bed material due to impingement of the jet is reduced significantly (Figure 4.2.2.1).

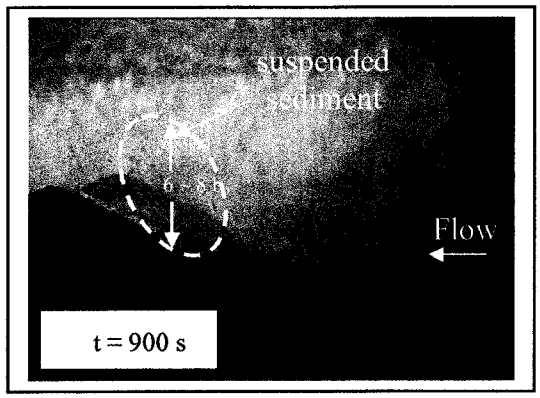

Figure 4.2.2.1: Suspended sand grains at t = 900 s

In this time zone, the sand particles are carried in the vertical direction up to about 6 ~ 8 b_o. It should be noted that the amount of suspended sand is well below the quantity

observed in time zone A. Two well defined concave shaped depressions stretching from the region C into region D (and from E to F) in Figure 4.2.1 are formed. One can also observe two or three longitudinal streaks, that form and disappear rapidly in the scour hole region. The presence of these streaks caused sand to be deposited as small longitudinal ridges. The streaks were very similar to that noticed by Hopfinger et al. (2004).

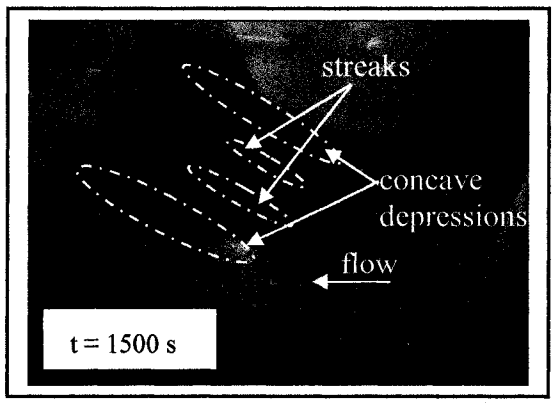

Figure 4.2.2.2: Fluid structures at t = 1500 s

Figure 4.2.2.2 shows the scour hole at t = 1500 s exhibiting two streaks and two concave depressions. Hopfinger et al. (2004) did not report the presence of these concave shaped depressions. One can note from Figure 4.2.2.2 that the concave depression on either side of the streaks are very prominent. The formation and disappearance of the streaks continued for a relatively significant period. Hopfinger et al. (2004) observed loose sediment streaks or longitudinal ridges on the positive bed slope in the scour hole while in the present tests, the streaks were observed mostly in the near-zero bed slope region and at the beginning of positive bed slope (see Figure 4.2.1 for definitions). Hopfinger et al. (2004) mentioned that these streaks or longitudinal ridges represented signatures of intense longitudinal vortices which lift up the sediment. They attributed these vortices to

Görtler instability and have shown that the flow conditions favour such instability. In the present tests, these systematic formations of loose streaks were not observed, although there was the tendency for the formation of one or two very unstable short streaks. It is important to point out that Hopfinger et al. (2004) conducted their experiments in the submergence range of 2.75 to 8.8, which is much lower than that used in the present study. Previous studies in this range of submergence noted the flow to be strongly influenced by flicking of the jet towards the bed and free surface in an alternate manner (Balachandar et al. 2000).

4.2.3 3 hrs ≤ t ≤ 24 hrs: (Time zone C)

After about 3 hours, when scour has progressed sufficiently, the streak-like features become less prominent. On either side of the flume axis, a 'scoop and throw' scouring action appears which causes longitudinal concave shaped depressions and is represented in Figure 4.2.3.1.

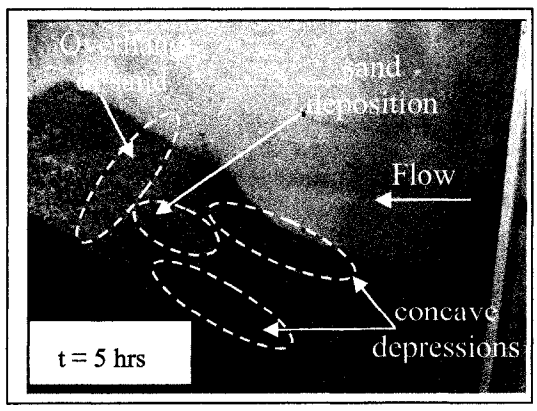

Figure 4.2.3.1: Longitudinal concave shaped depressions at t = 5 hrs

This is once again in the region C-D and E-F in Figure 4.2.1. Some of the sand particles are fluidized at the end of these concave shaped depressions and are carried by the flow downstream into the mound region. A portion of the sand particles accumulate on the upstream face of the mound and between the two concave shaped depressions. These eventually slide back into the depressions when apparently their weight is greater than the sweeping force of the scour action. The 'scoop and throw' action is then momentarily halted. One can also observe a lifting spiraling motion of sand particles near the end of the concave shaped depression, indicative of some type of vortex activity. Dye visualization in the near bed region confirms vortex-like structures and the sudden acceleration of the flow at the end of the scooped region. One can also confirm the presence of the vortices by observing the motion of individual sand grains.

4.2.4 24 hrs $\leq$ t $\leq$ 72 hrs: (Time zone D)

The 'scoop and throw' scouring action slowed down after 24 hours. The scouring process continues, but at a relatively slower pace. The concave shaped depression caused by the 'scoop and throw' mechanism is not that apparent at this stage but small scale suspension of bed material provides the evidence of 'scoop and throw' action. One can notice small scale bed suspension on one side of the flume axis in Figure 4.2.4.1 (which shows only the near-bed region).

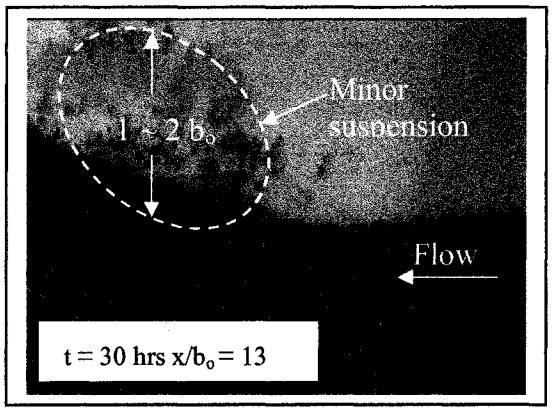

Figure 4.2.4.1: Small scale suspension near the bed

The suspension of a very few sand grains extends to about 1 ~ 2 b_o. The progress of the scour hole continues up to 72 hrs, though with reduced intensity in the 'scoop and throw' action. Dye injection confirmed the presence of spiral motions during this time period. Figures 4.2.4.2 to 4.2.4.5 show images of the flow field with dye in the near-bed region at x/b_o = 10. The dye is injected by an L-shaped tube with the exit port facing the near wall of the flume. In Figure 4.2.4.2, the dye initially flows towards the near side wall (i.e., out of the picture) and spirals towards the upstream direction.

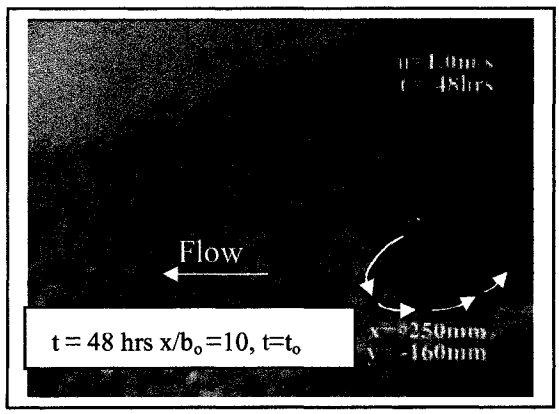

Figures 4.2.4.2: Dye flow towards side wall at 48 hrs, t = t_o s

In Figure 4.2.4.3, the dye injection is shown 2 s later than that in Figure 4.2.4.2. The dye now exits the port and flows towards the far wall.

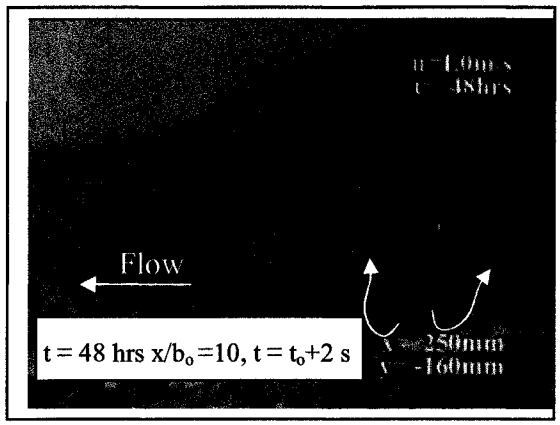

Figures 4.2.4.3: Dye flow towards far wall at 48 hrs, $t = t_o + 2$ s

In Figure 4.2.4.4 (acquired 4 s later than Figure 4.2.4.3), the dye flows downstream at a slight angle to the streamwise direction.

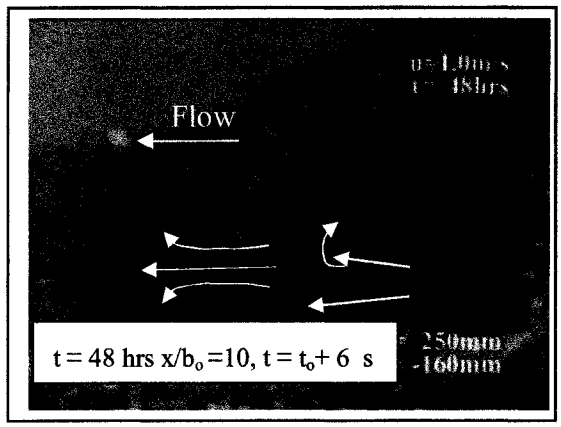

Figure 4.2.4.4: Dye flow downstream at 48 hrs, $t = t_o + 6$ s

Collectively, using images such as Figures 4.2.4.2 to 4.2.4.4 and several video frames, a clear spiraling motion can be deciphered.

4.2.5 t > 72 hrs: (Time zone E)

About 72 hours into the scour process, when the scour hole attained a near asymptotic state, what can be described as turbulent bursts were noticed to occur in the near-bed regions across the cross-section of the flume. Figures 4.2.5.1 and 4.2.5.2 show images with and without turbulent bursts separated by a time of 2 s.

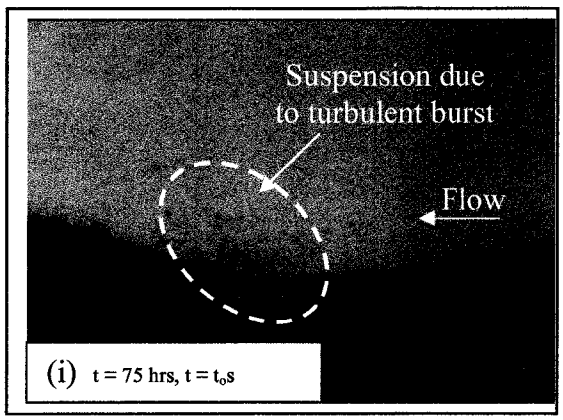

Figure 4.2.5.1: Turbulent burst at 75 hrs, t = t_o s

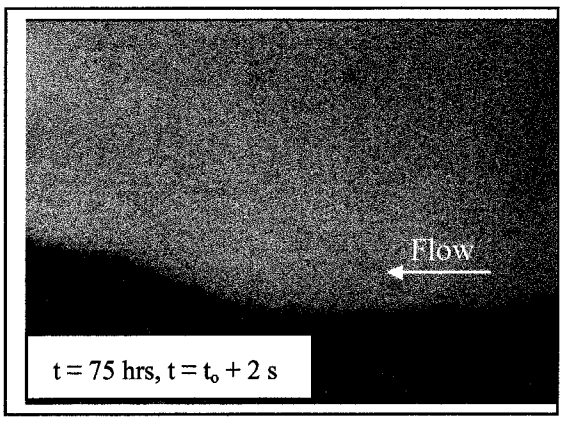

Figure 4.2.5.2: Bed region 2 s after Figure 4.2.5.1

The effect of the burst can be noticed by the suspension of sand particles. These bursts were frequent and occurred randomly. Furthermore, they caused the movement of sand particles close to the bed region in all directions. The transport in the vertical direction is

less than b_o ($\approx$ 25 mm). This type of activity is visible in a section beyond the maximum scour hole location (Figure 4.2.1). In addition, at asymptotic conditions, two prominent scour mechanisms were observed to occur on either side of the flume axis, as shown in Figure 4.2.5.3.

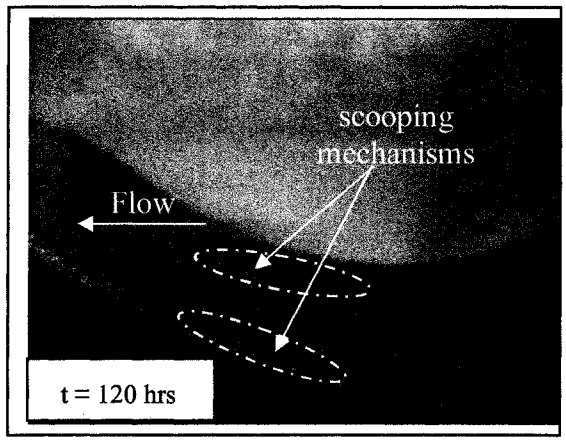

Figure 4.2.5.3: Scooping mechanisms at t = 120 hrs

As a consequence of these mechanisms, sand particles were laterally moved from the region. Particles appeared to be spiraled towards the side walls and the flume axis. These two scour mechanisms occurred quite frequently and as measured by the movement of sand particles, the two fluid structures causing the scour appear to be identical in strength as the bed contour was symmetrical about the flume axis. Occasionally, one would note that one of the two structures was stronger than the other, and this caused lateral movement towards the weaker side. This momentarily caused the bed contour to become asymmetrical. No preferential occurrence on one or the other side of the flume axis of the stronger structure was noted. It should be remarked that at asymptotic conditions, the back and forth movement of the impingement point (discussed in the next section), the

frequent but random turbulent bursts and the two prominent scour mechanisms, all occurred at one time or the other. The jet impingement tends to cause a limited suspension and lifting of the sand particles into the flow stream where they are picked up and transported by the higher velocity fluid parcels. In addition, the fluid structures caused vigorous lateral movement. It is however noteworthy that in spite of these actions, any changes in the instantaneous bed profile was a local phenomenon and did not cause significant change in the overall mean bed profile. There is also no large scale movement of bed particles anywhere within the flow field. It should also be noted that at the asymptotic state, scour profile in the hole region is nominally two-dimensional across the width of the flume. However, at the mound region, the lateral profile is not two-dimensional and has two distinct peaks (Region G and I of Figure 4.2.1). These peaks occur closer to the side walls leaving a trough in the centre portion of the mound (Region H of Figure 4.2.1). This was also noticed in an earlier study (Deshpande 2004).

4.3 Jet Impingement

During the progress of the scour hole, visual observation indicates that the jet impingement point moves back and forth, as has been observed by Deshpande (2004). This can be confirmed by the presence of upstream and downstream movement of sand particles near the bed in the range $0 < x/b_o \leq 16$. Figure 4.3.1 shows the histogram of streamwise velocity along the scour bed for Test B at various locations ($10 < x/b_o \leq 20$).

These locations extend from the end of the negative bed slope region to the start of the positive bed slope region as indicated in Figure 4.3.1b. One can note from these figures that, for $10 < x/b_o \leq 13$ (Figure 4.3.1a, Figure 4.3.1c to Figure 4.3.1e), although the streamwise mean velocity is very low near the bed, the instantaneous velocity varies in a wide range from -0.8 m/s to 1.0 m/s. The histogram has two distinct peaks and one can also note that the negative instantaneous velocity count is more than 57 %, which is a clear indication of back and forth movement of the jet impingement point. For $x/b_o \geq 14$ (Figures 4.3.1f to 4.3.1h), the value of mean streamwise velocity increases and the negative instantaneous velocity count decreases. For the location of $x/b_o = 20$ (Figure 4.3.1i), the negative instantaneous velocity count is less than 10% and the overall histogram tends to have a single peak with more turbulence-like fluctuations rather than back and forth jet movement. This is an indication that the jet impingement point extends up to about $x/b_o \approx 18$ with a mean location (defined as the location where 50% of velocity realizations are negative) occurring around $x/b_o \approx 13$.

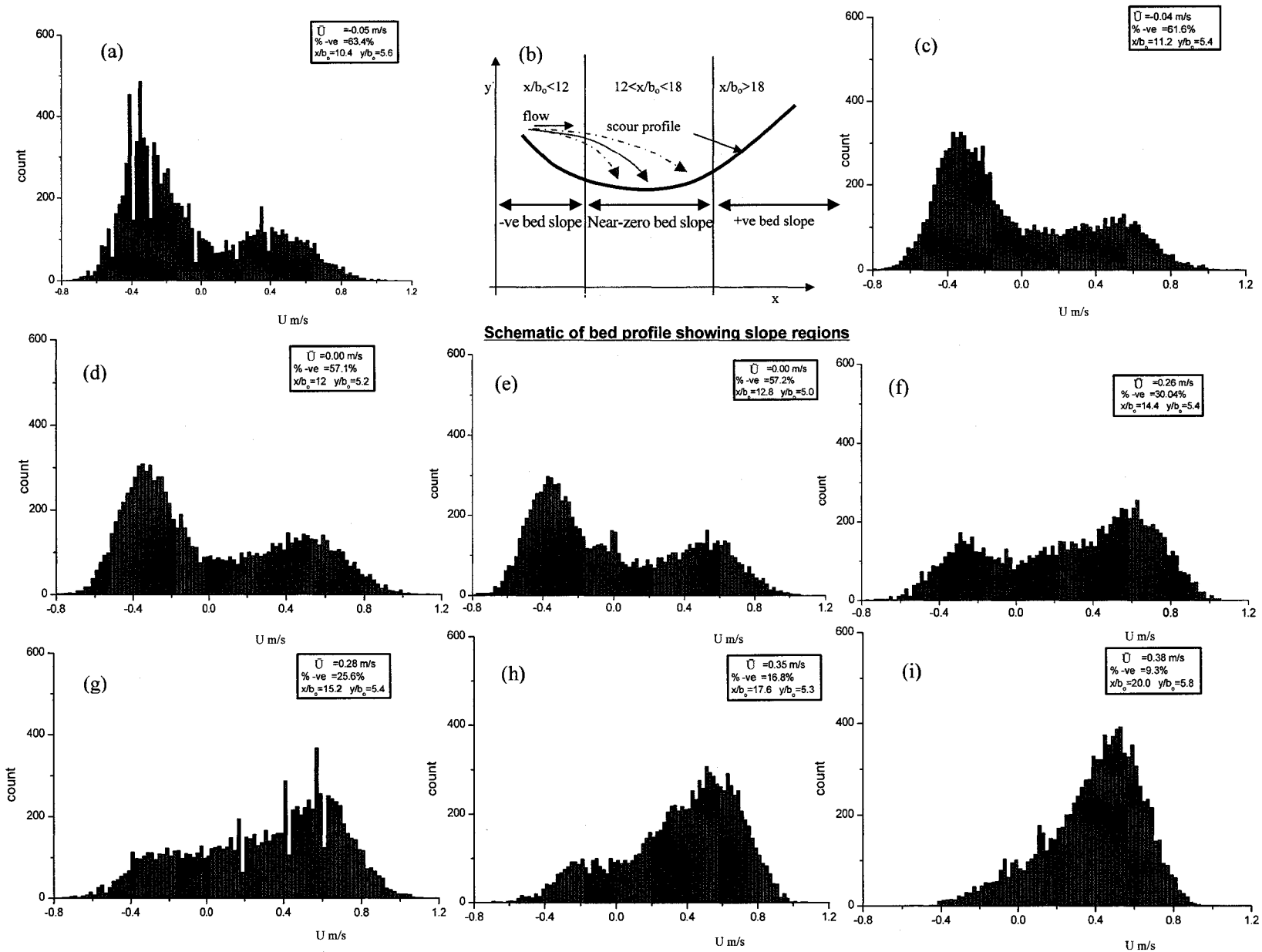

Figure 4.3.1: Histogram of streamwise velocity distributions along the scour bed for Test B

4.4 Mean Velocity Profiles

Figure 4.4.1 shows velocity vector plots in the scour hole region at asymptotic conditions for Test A. One can clearly see from the vector plots that the jet expands and interacts with the bed. As can be clearly seen in Test A, in the region above the jet, there is a large scale recirculating region which extends to about $30b_0$ downstream. The centre of this region is located at about $16b_0$ along the x axis and about $10b_0$ along the y axis. It is important to recognize that this recirculation region provides for significant downward directed velocity component near the nozzle. The impingement of the jet also generates a recirculating flow in the bed region close to the nozzle. A similar velocity plot was obtained for Test B and is shown as Figure 4.4.2. The plot here does not cover the entire flow region. After three experimental runs of Test A and obtaining similar velocity patterns in Test B in both streamwise and normal to the undisturbed bed profile directions as shown in Figures 4.4.5 and 4.4.9 respectively, it was observed that the plot for Test B was qualitatively similar to that obtained in Test A.

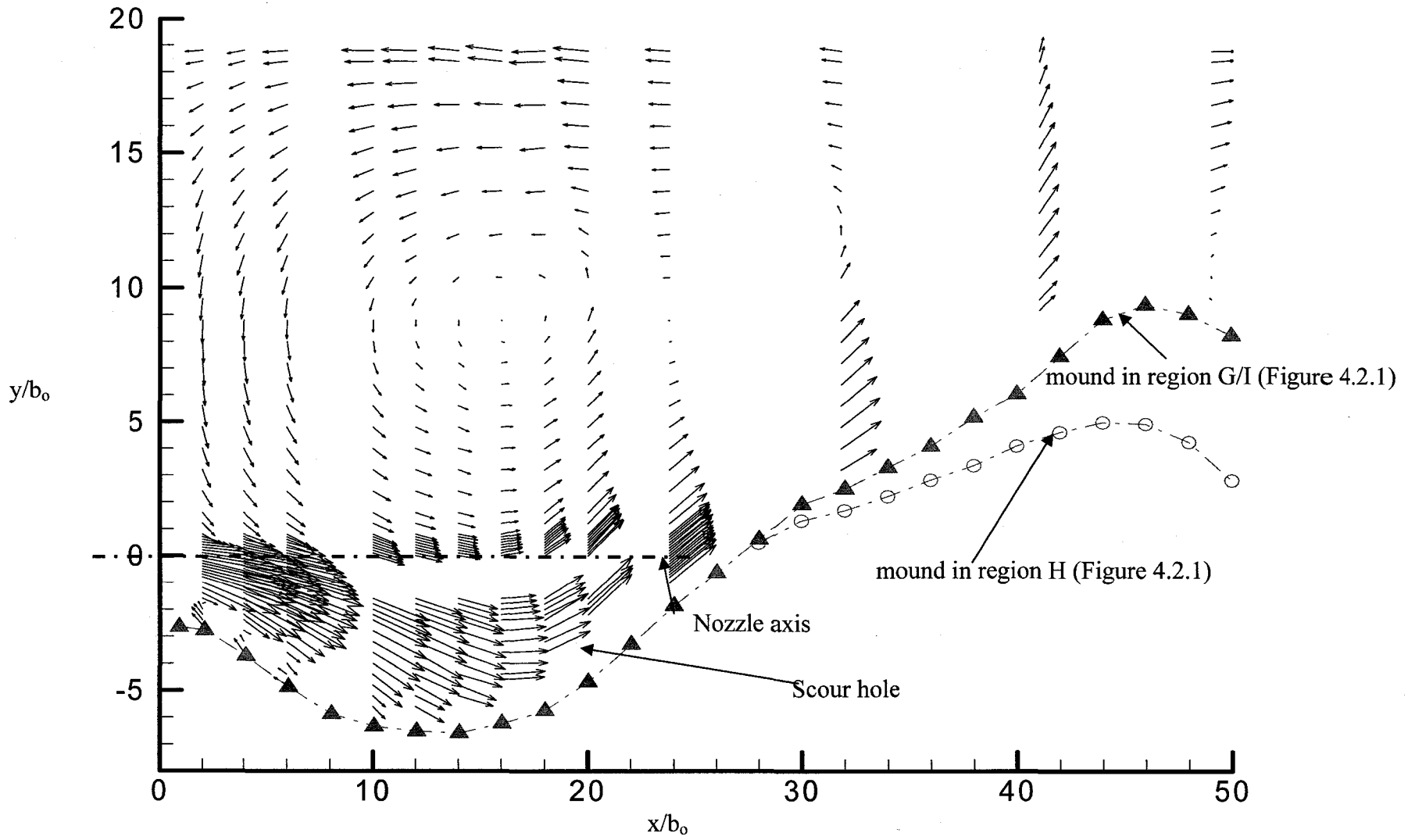

Figure 4.4.1: Velocity vector plot for Test A

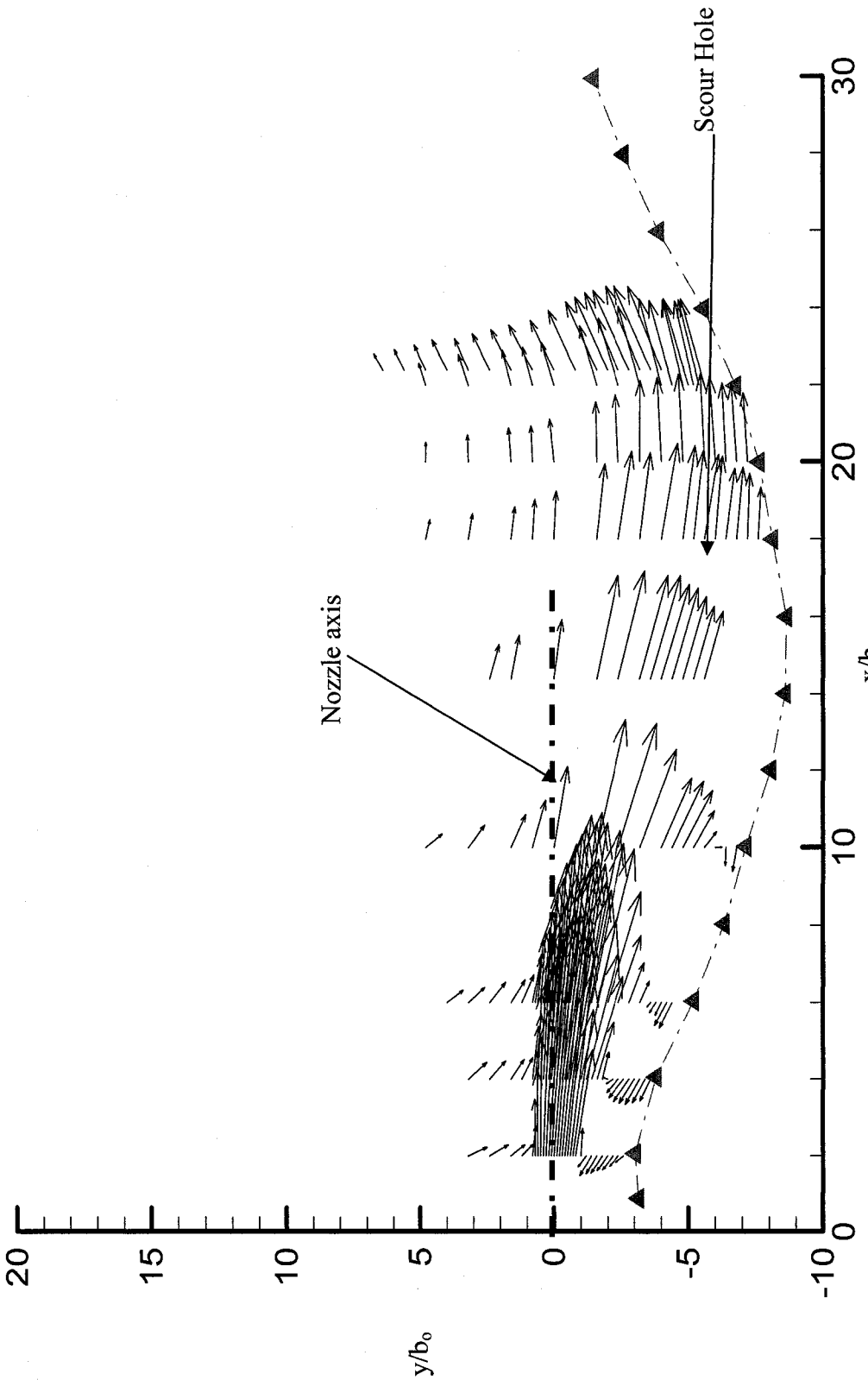

Figure 4.4.2: Velocity vector plot for Test B

Figures 4.4.3 and 4.4.4 show the streamwise mean velocity profile for Test A and Test B respectively at various stations along the nozzle axis in the scour hole region. The mean velocity is normalized by the jet velocity U_o. In progressing from near the nozzle to several downstream stations, the jet expands. The locus of the maximum velocity (inset in Figure 4.4.3a) shifts downwards away from the nozzle axis which is indicative of the jet bending. The expansion is indicated by the jet half-width in Figure 4.4.3j. Clearly, the jet expands asymmetrically and the rate of expansion is higher than free jets. The bottom half of the jet displays a greater half-width than the upper half of the jet. Moreover, it is clear from Figure 4.4.3j and the inset in Figure 4.4.3a, the jet characteristics are different from a free jet. This is different from the observation of Rajaratnam and Berry (1977) who noted the jet characteristic to be similar to a free jet up to the point of maximum scour. For $y/b_o > 10$, (Figure 4.4.3) the velocity is negative at all stations shown in Figures 4.4.3 and 4.4.4. For convenience of description, the flow can be divided into three zones. Figures 4.4.3a to 4.4.3c and 4.4.4a to 4.4.4c for Tests A and B respectively, describe the profiles along the region of negative bed slope (see region A and B in Figure 4.2.1). Figures 4.4.3d to 4.4.3g for Test A and Figures 4.4.4d to 4.4.4g for Test B provide the results in the region of near-zero bed slope (see region C and E in Figure 4.2.1) and Figures 4.4.3h and 4.4.3i, and 4.4.4h and 4.4.4i for Tests A and B respectively describe the velocity profiles in the region of positive bed slope (see region D and F in Figure 4.2.1). One can observe that the value of $\overline{U}$ is negative near the sand bed for the region with negative bed slope (Figures 4.4.3a to 4.4.3c (Test A), Figures 4.4.4a to 4.4.4c (Test B)) indicating reverse flow condition for this region.

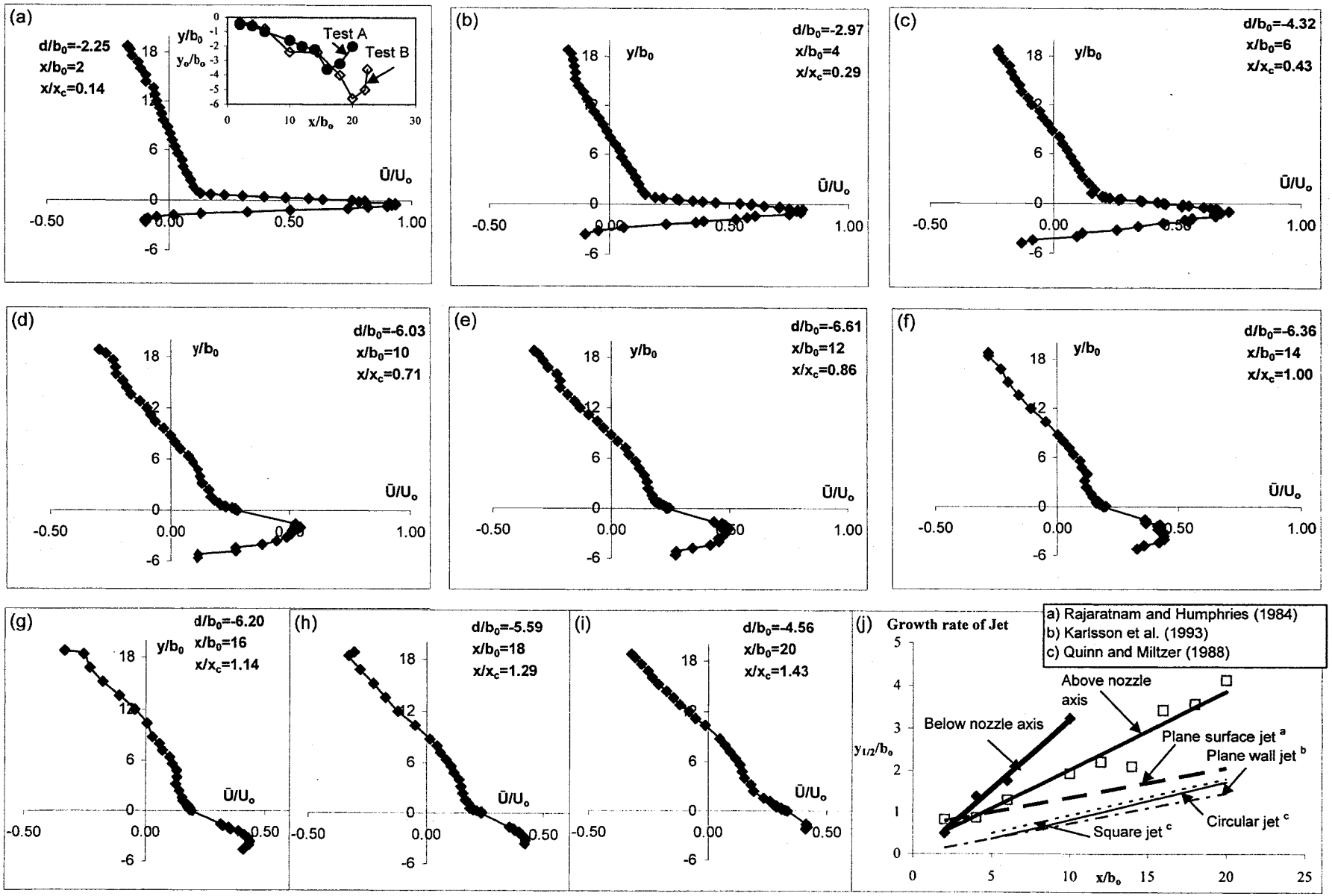

Figure 4.4.3: Streamwise mean velocity profiles at various axial stations for Test A

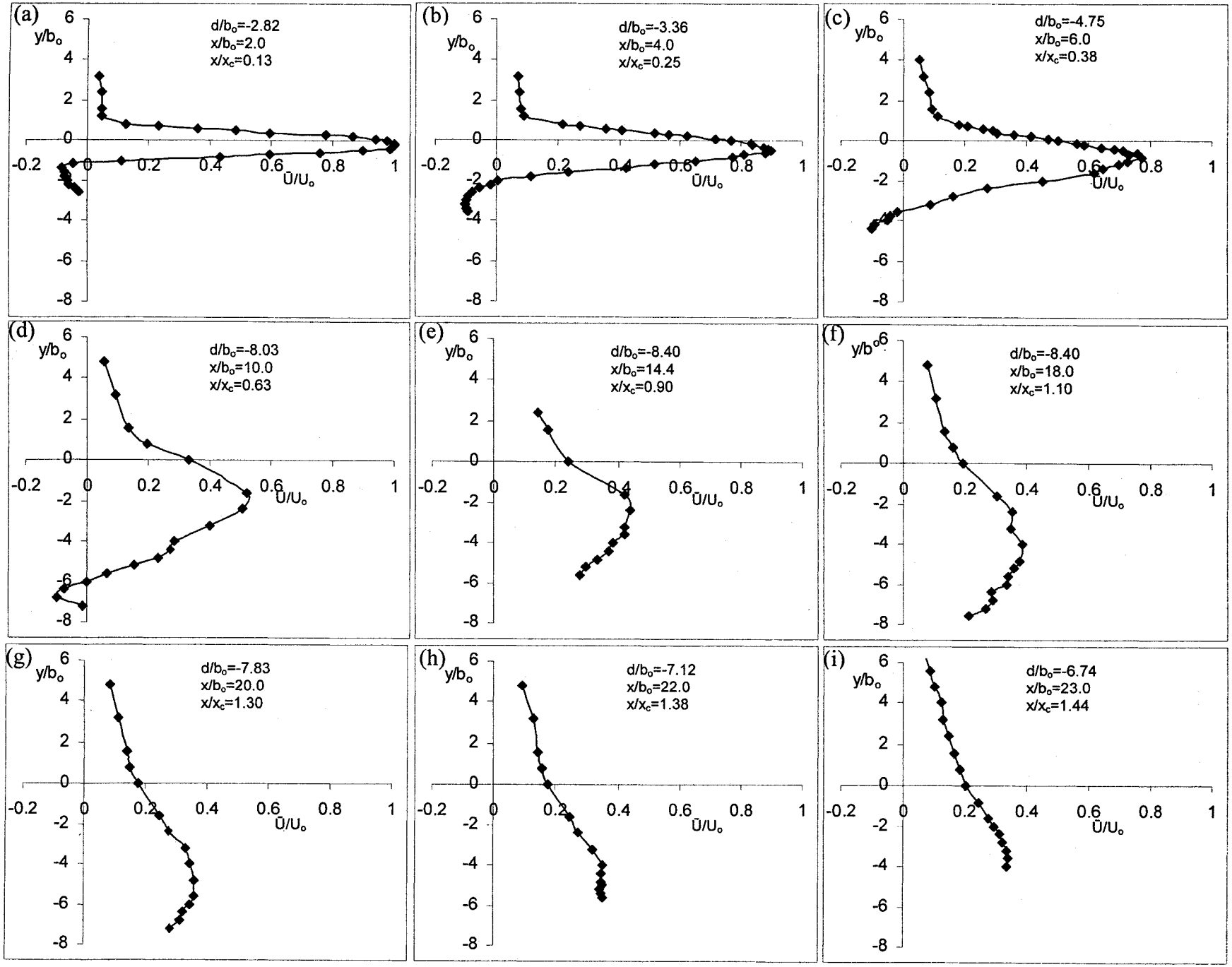

Figure 4.4.4: Streamwise mean velocity profiles at various axial stations for Test B

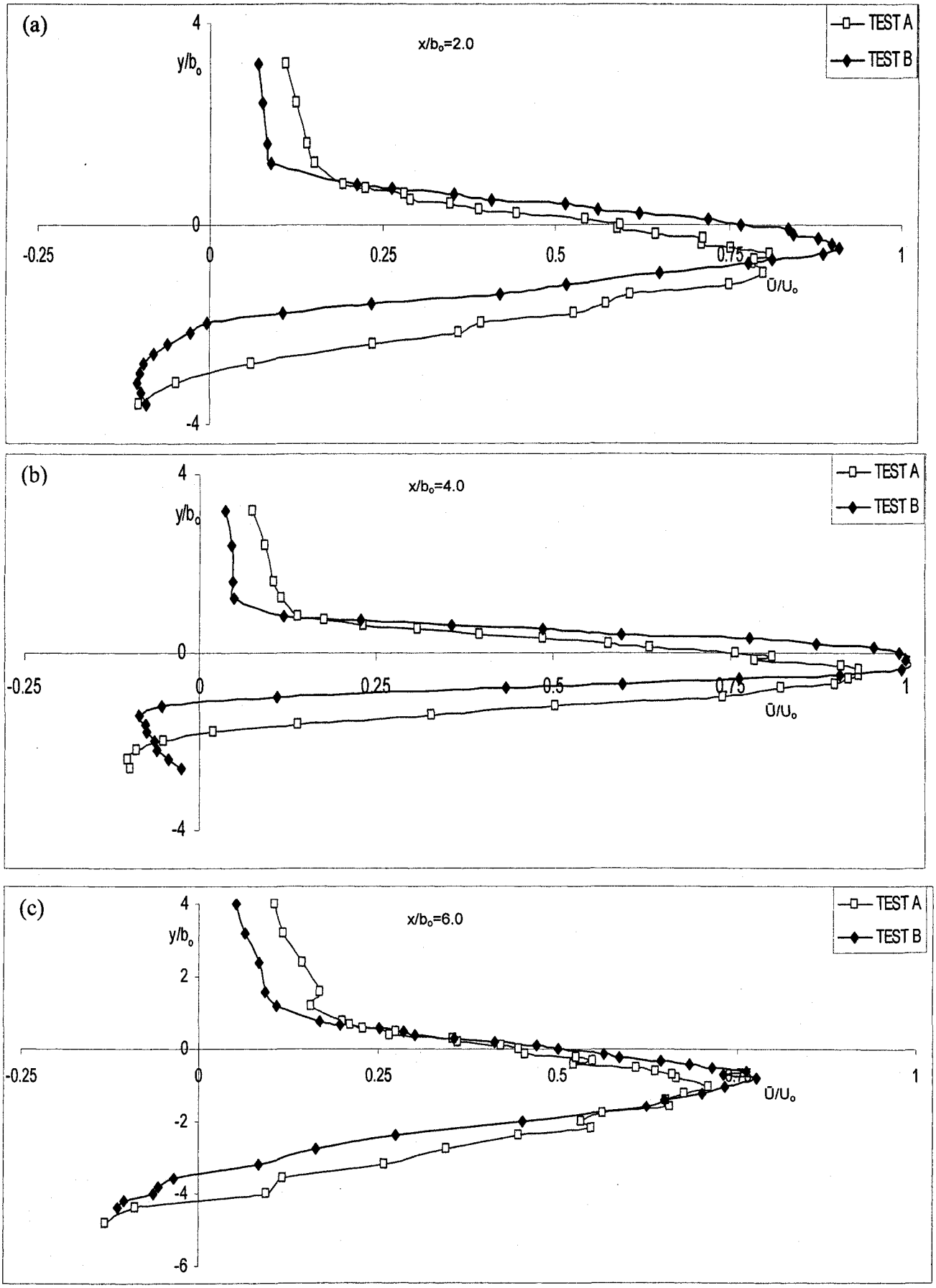

Figure 4.4.5: Comparison of streamwise mean velocity profiles for Tests A and B for $2 \leq x/b_o \leq 6$

The value of $\overline{U}$ is positive near the sand bed for the region with near-zero slope (Figures 4.4.3d to 4.4.3g (Test A), 4.4.4d to 4.4.4g (Test B)). From visual observations, one can notice vigorous sand movement in this region. In Figures 4.4.3h and 4.4.3i, and 4.4.4h and 4.4.4i, for Tests A and B respectively, the maximum velocity does not change much as the flow begins to climb up the scour hole on the downstream scour hole slope.

Figure 4.4.6 shows the mean velocity profiles for $x/x_c > 0.7$ using wall jet scaling. Here, $y_{½}$ refers to the jet half width and U_{max} is the maximum streamwise velocity at any station. Clearly, the present data in the near-zero bed slope region describes a plane wall jet as indicated by the comparison with a set of wall jet data (Tachie, 2000). However, farther away ($x/x_c = 1.7$), the present data deviates from a plane wall jet while negotiating the wall curvature.

Figures 4.4.7 and 4.4.8 show the mean velocity $\overline{V}$ profiles in the vertical direction for Tests A and B respectively at various stations along the nozzle axis. Figures 4.4.7a to 4.4.7c (Test A), and 4.4.8a to 4.4.8c (Test B) shows the $\overline{V}$ profile along the region of negative bed slope. One can note that the value of $\overline{V}$ is positive near the sand bed and for the same locations the value of $\overline{U}$ was negative (Figures 4.4.3a to 4.4.3c for Test A and Figures 4.4.4a to 4.4.4c for Test B), indicating reverse flow directed slightly upwards. Away from the bed, $\overline{V}$ is negative due to the jet bending towards the sand bed. If the jet had free jet characteristics, one would have expected the value of $\overline{V}$ to be positive above the jet centreline due to expansion. Clearly, in Figures 4.4.7a to 4.4.7c and 4.4.8a to 4.4.8c, for Tests A and B respectively, the values of $\overline{V}$ are negative above the point of

maximum streamwise velocity with a tendency to decrease towards zero. The large recirculating flow above the jet contributes to significant downward flow (Figures 4.4.1 and 4.4.2 for Tests A and B respectively) and thereby influences the mean values of $\overline{V}$. Figures 4.4.7d to 4.4.7g (Test A) and Figures 4.4.8d to 4.4.8g (Test B) show the variation of $\overline{V}$ along the region of near-zero bed slope. One can note that the value of $\overline{V}$ is negative near the sand bed and for the same locations the value of $\overline{U}$ is positive (Figures 4.4.3d to 4.4.3f and Figures 4.4.4d to 4.4.4f for Tests A and B respectively), indicating flow impingement. One can also note that the negative value of $\overline{V}$ reduces and becomes positive as the jet reaches near the end of near-zero bed slope (Figure 4.4.7g, (Test A) and Figure 4.4.8g (Test B)). This is the indication that the jet tends to follow the bed slope. Figures 4.4.7h and 4.4.7i and Figures 4.4.8h and 4.4.8i for Tests A and B respectively shows the variation of $\overline{V}$ along the region with positive slope. One can observe that the value of $\overline{V}$ is positive near the sand bed and the value of $\overline{V}$ increases with the increase of distance from the nozzle, indicating flow acceleration along the positive scour slope. It can be seen that $\overline{V}$ is negative up to $x/b_o = 14$, indicating that the tendency to impinge continues up to this station.

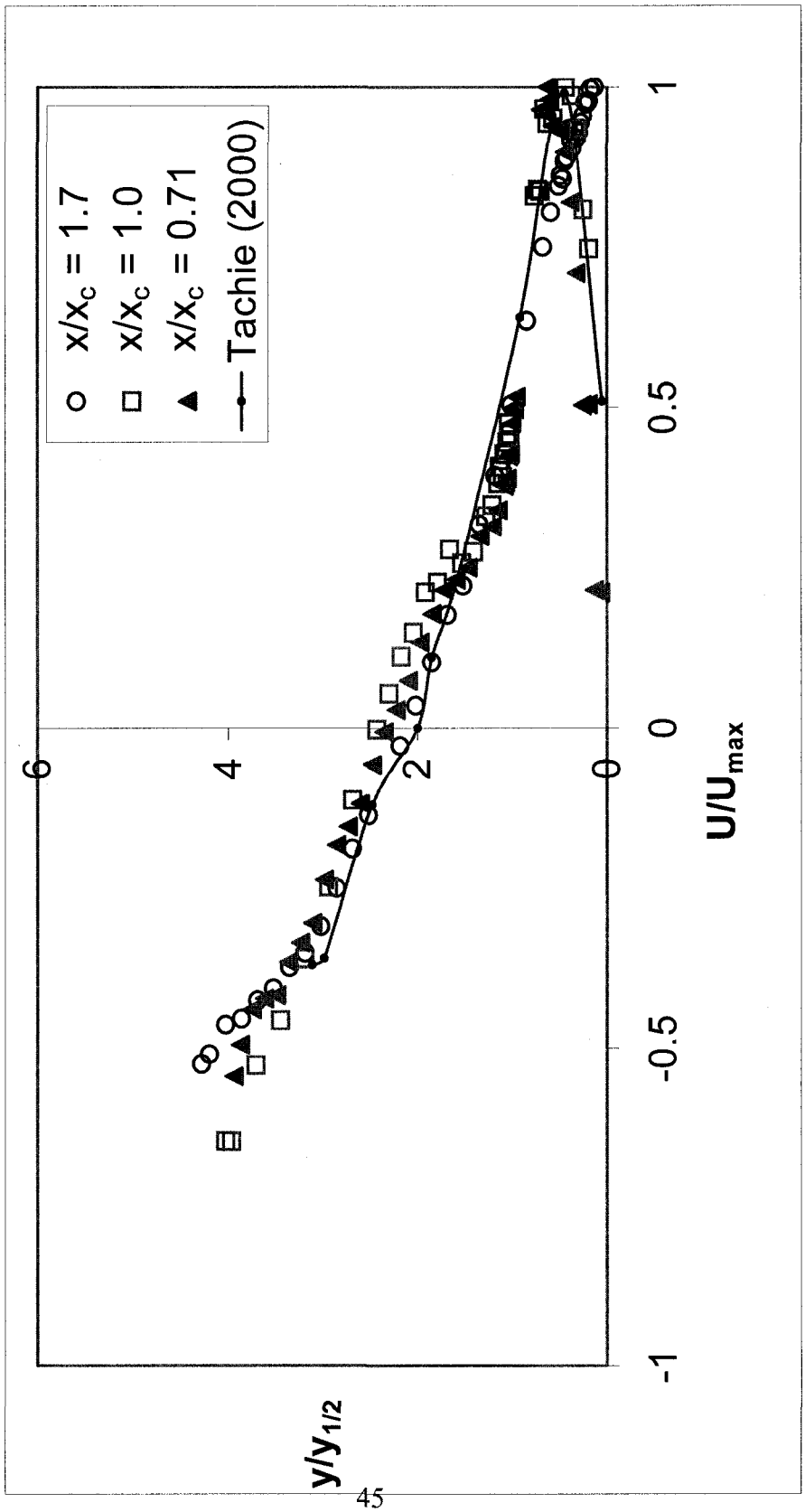

Figure 4.4.6: Streamwise velocity profiles in wall jet scaling

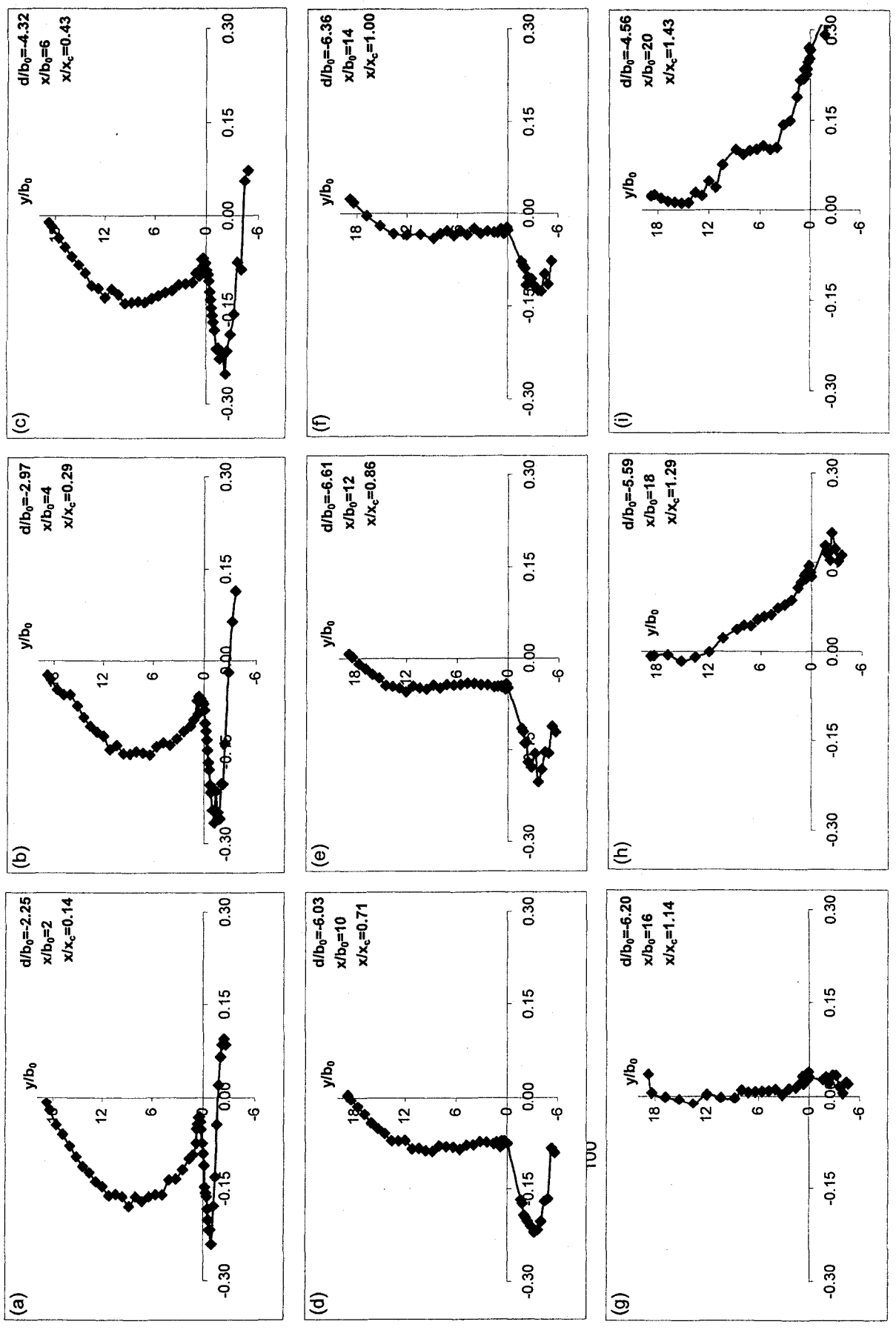

Figure 4.4.7: Velocity profiles normal to the initial bed at various axial stations for Test A

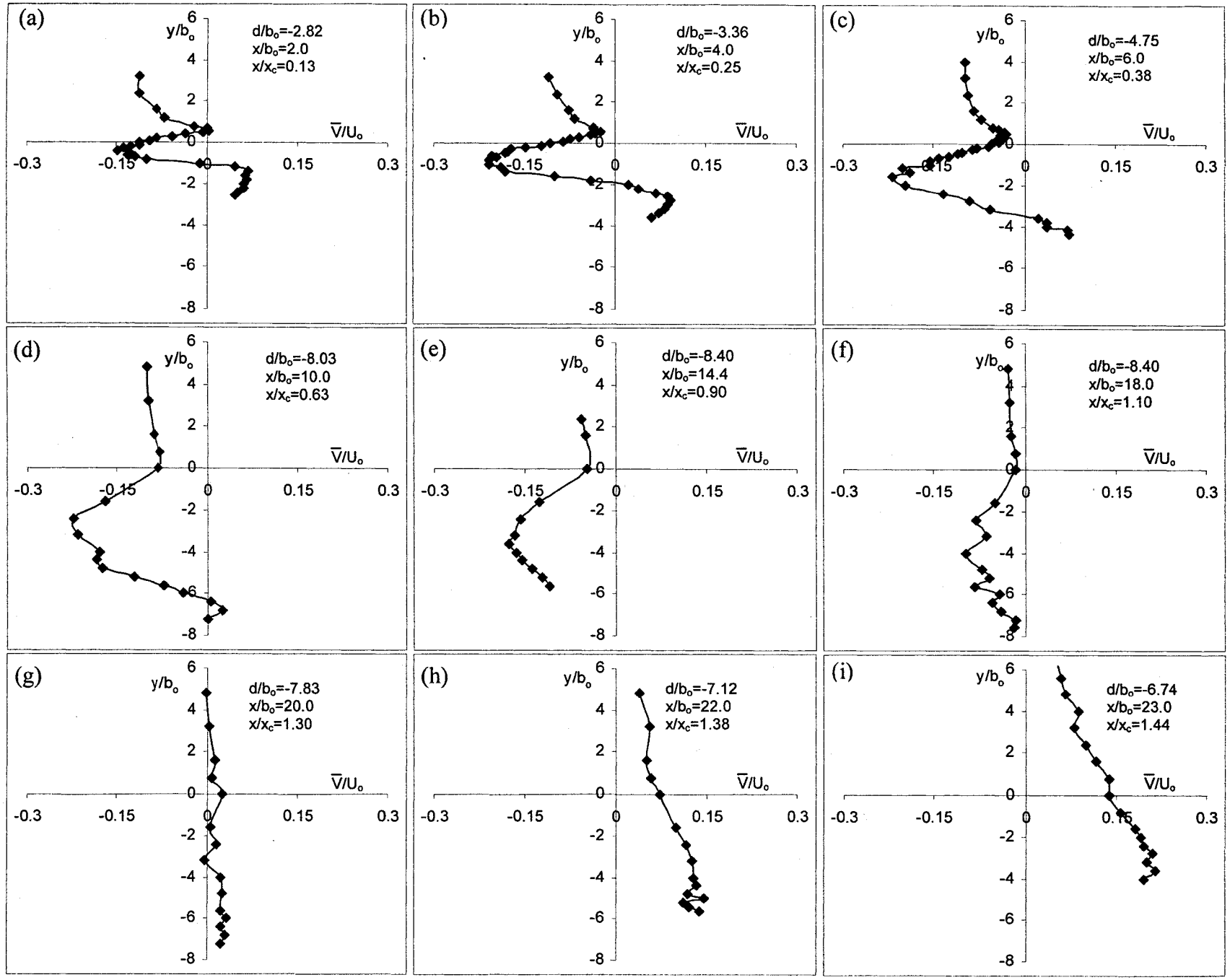

Figure 4.4.8: Velocity profiles normal to the initial bed at various axial stations for Test B

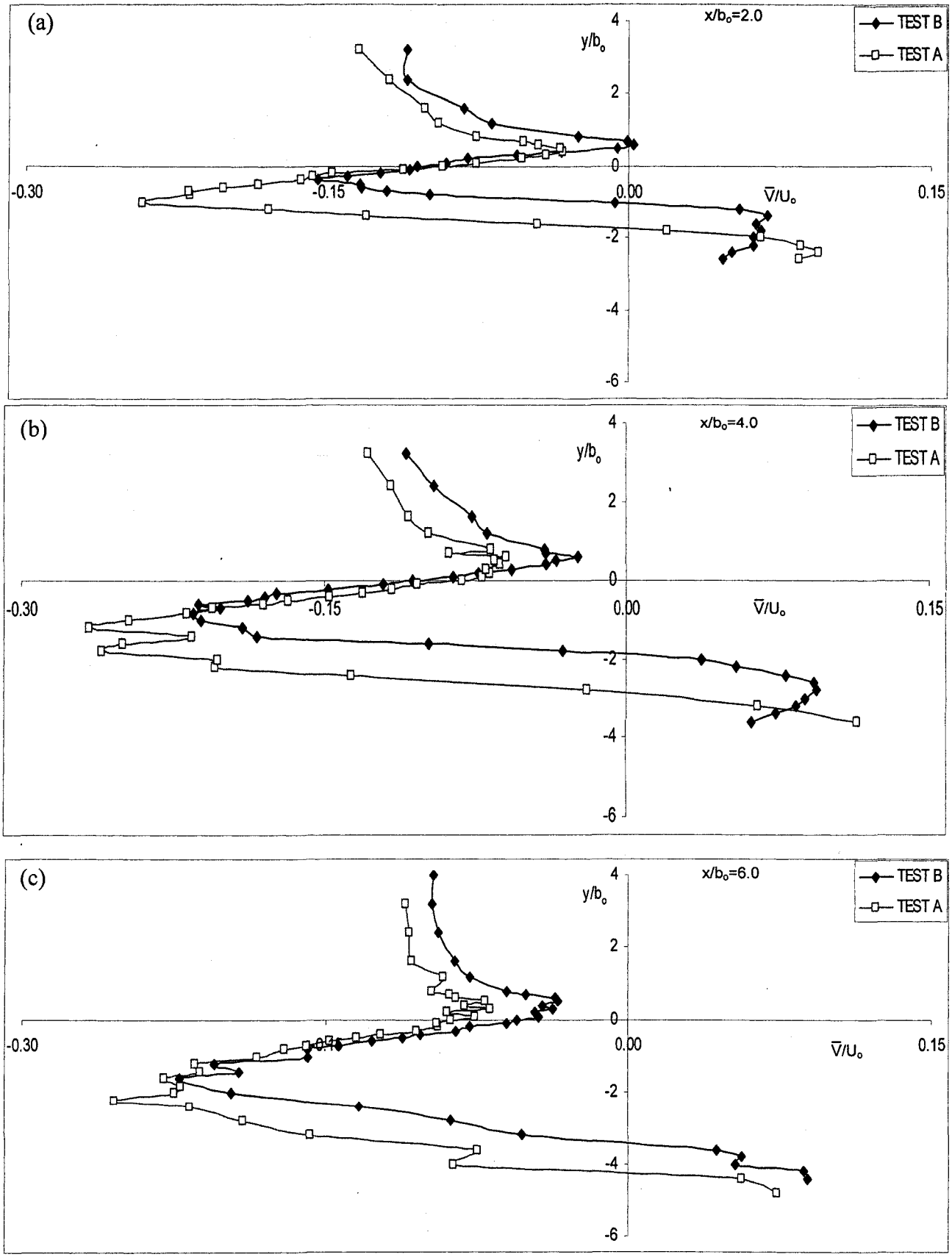

Figure 4.4.9: Comparison of velocity profiles normal to the initial bed for Tests A and B for $2 \leq x/b_o \leq 6$

4.5 Higher Order Moments

Figures 4.5.1 and 4.5.2 shows plots of the streamwise turbulent intensity, $\overline{u^2}$, and the turbulent intensity normal to the initial bed, $\overline{v^2}$, for Test A and Test B, respectively. At the various axial stations near the nozzle ($x/b_o < 6$), there is a tendency to have two distinct peaks, mainly caused by the entrainment of the fluid from above and below the jet. This is typical of a two-dimensional jet entering an ambient flow. However, in the present flow field, the peak near the bed is consistently higher. The asymmetry about the jet centreline is a clear deviation from free jet conditions. This is a consequence of the local turbulence generated due to the interaction of the sand and the fluid in addition to the turbulence generated by entrainment effects. The bottom peak tends to get larger in Figures 4.5.1d and 4.5.2d. The remnants of the turbulence generated earlier are still prevalent at $x/b_o = 14$, ($x/x_c \approx 1$) (Figures 4.5.1f and 4.5.2f).

Beyond the maximum depth of scour ($x > x_c$), the mean flow is locally accelerating and the overall turbulence intensity decreases. One can note a similar distribution in the $\overline{v^2}$ profiles. The location of the maximum peak in the $\overline{u^2}$ and $\overline{v^2}$ profiles occur at the same value of y/b_o for the negative bed slope region. For these stations the values of $\overline{u^2}$ are greater than the value of $\overline{v^2}$. It should be noted that the second peak in the $\overline{v^2}$ profiles which occurs farther away from the sand bed, diminishes with increasing distance from the nozzle and is non-existent for $x/x_c > 0.7$. For the positive bed slope region, one can note that the value of $\overline{v^2}$ tends to be more than the value of $\overline{u^2}$ and the increases with increasing downstream distance.

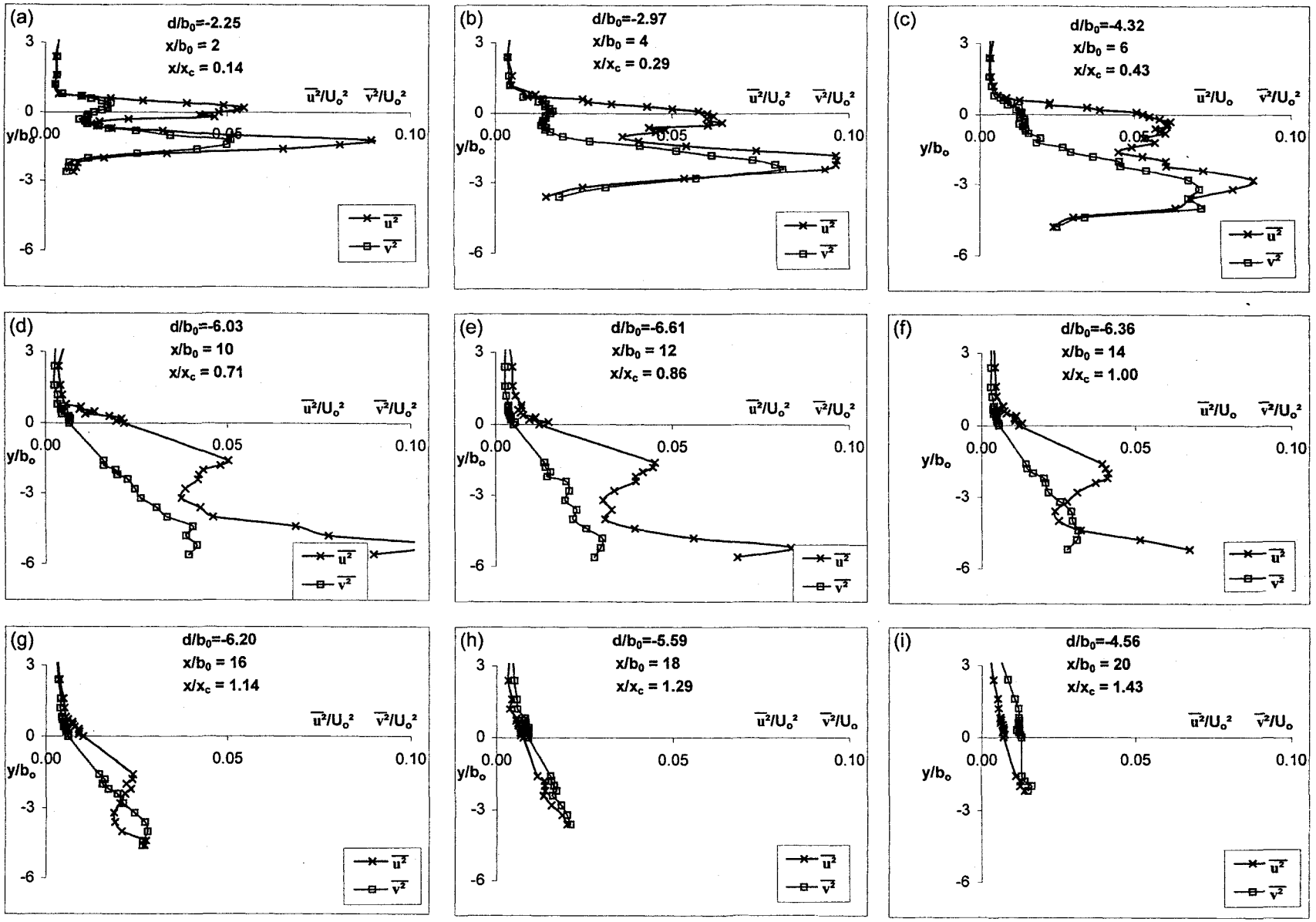

Figure 4.5.1: Streamwise turbulent intensity and the turbulent intensity normal to the initial bed at various axial stations for Test A

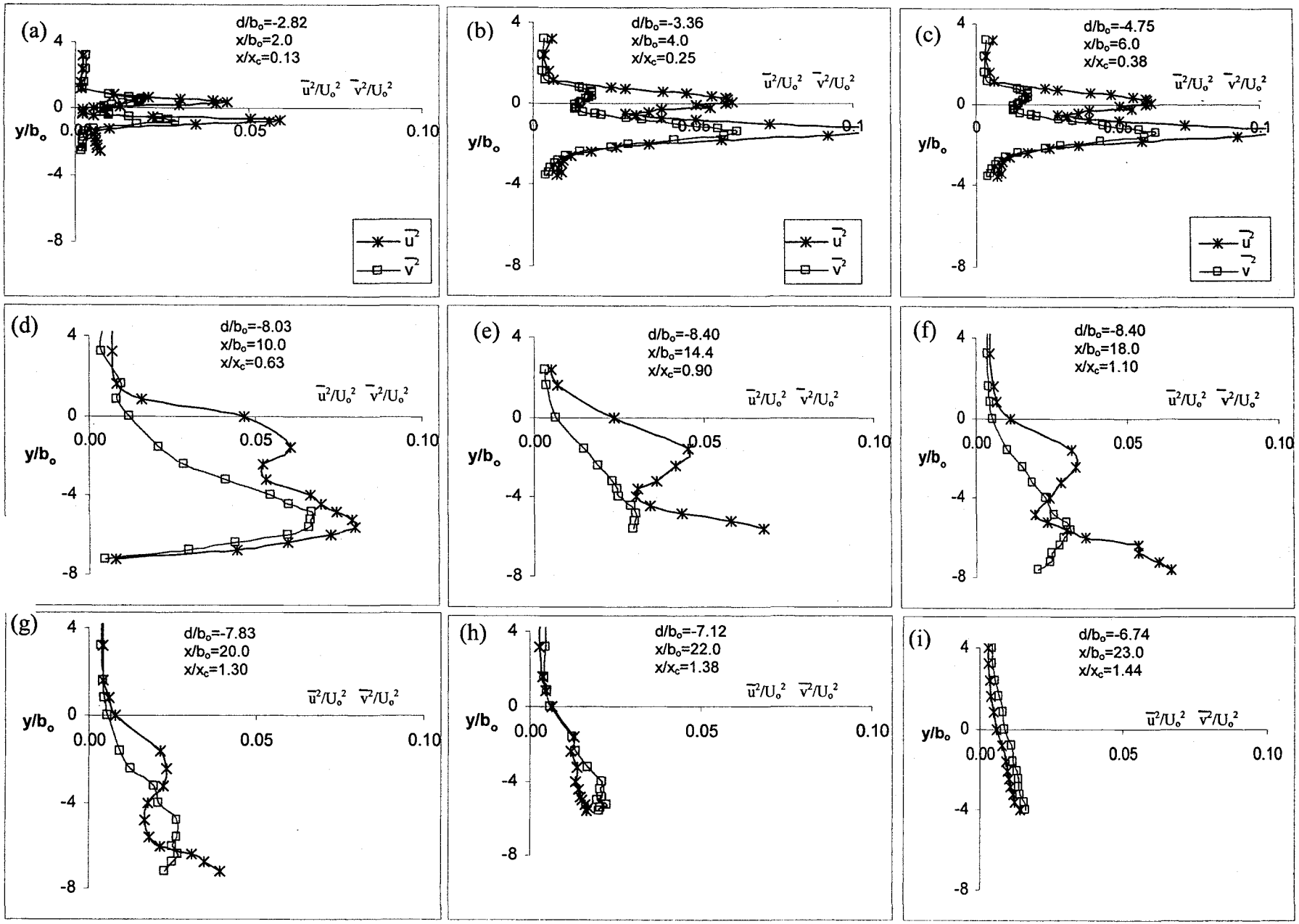

Figure 4.5.2: Streamwise turbulent intensity and the turbulent intensity normal to the initial bed at various axial stations for Test B

Figure 4.5.3 shows the turbulent shear stress profile at three locations corresponding to the three bed slope regions. The data for the two tests corresponding to nearly identical locations based on x/x_c is shown in each of the graphs in Figure 4.5.3. In the negative bed slope region, the peak in the profile for test A is closer to the bed while in the region of $x/x_c = 1$, the peak in the profile for test B is closer to the bed. Though the two tests are qualitatively similar, it should be remarked that the size of the scour hole in Test B is larger.

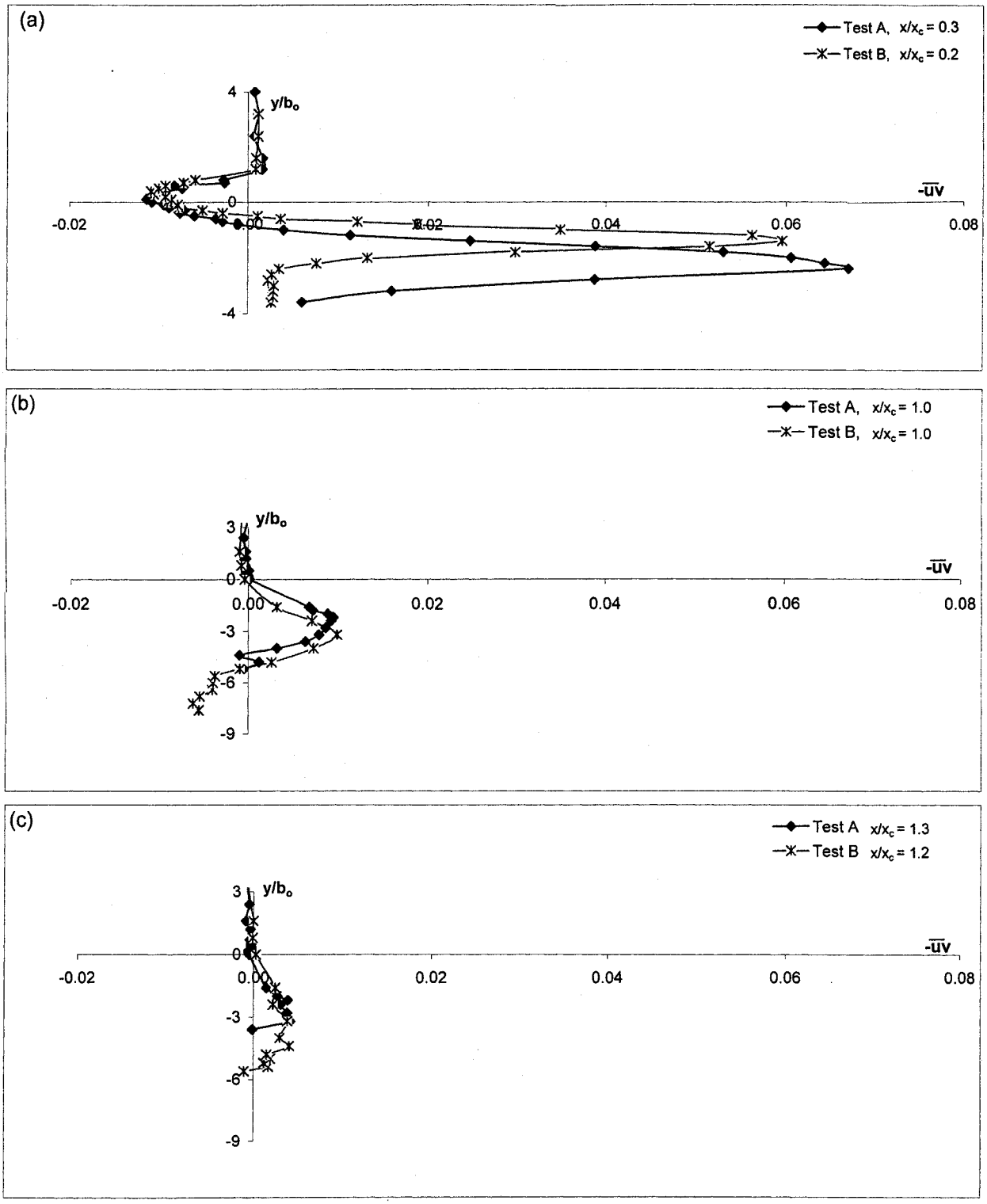

Figure 4.5.3: Turbulent shear stress profile at various axial stations

Figures 4.5.4 and 4.5.5 show the variation of turbulent diffusion in the y direction, $D_v = \overline{u^2 v}$ and the variation of $\overline{u^3}$, which can be thought of as the streamwise flux of the turbulent kinetic energy $\overline{u^2}$ at various axial stations for Test A and Test B respectively. For Tests A and B, the values for $\overline{u^2 v}$ and $\overline{u^3}$ above $y/b_o = 3$ are close to zero and therefore makes no significant contribution to the discussion on the effect of turbulence on scour. The nine sets of profiles in both tests are once again divided into 3 rows, depending on the location with respect to the maximum scour depth. Figures 4.5.4a to 4.5.4c and Figures 4.5.5a to 4.5.5c for Tests A and B respectively are in the region of negative bed slope, Figures 4.5.4d to 4.5.4g for Test A and Figures 4.5.5d to 4.5.5g for Test B are in the region of near-zero scour slope, whilst Figures 4.5.4h to 4.5.4i and Figures 4.5.5h to 4.5.5i for Tests A and B respectively are in the region of positive bed slope. Figure 4.5.4a (Test A) and Figure 4.5.5a (Test B) shows the variation of D_v and $\overline{u^3}$ at the location $x/b_o = 2$. At this location, the sand bed is at a vertical distance of $d/b_o = -2.25$ from the nozzle axis in Test A and $d/b_o = -2.82$ in Test B. One can note from the plot of both tests that both D_v and $\overline{u^3}$ are close to zero near the sand bed. As one progresses from the bed towards the free surface, absolute values of both D_v and $\overline{u^3}$ increase and attain local peaks at almost the same level ($y/b_o = -1.6$) but with opposite signs. D_v has a negative peak whereas $\overline{u^3}$ has a positive peak. The peak value of $\overline{u^3}$ is larger than that of D_v. This indicates strong sweeping motion in the flow direction that is partly directed towards the bed. If one were to extrapolate this flow process to earlier time periods, these

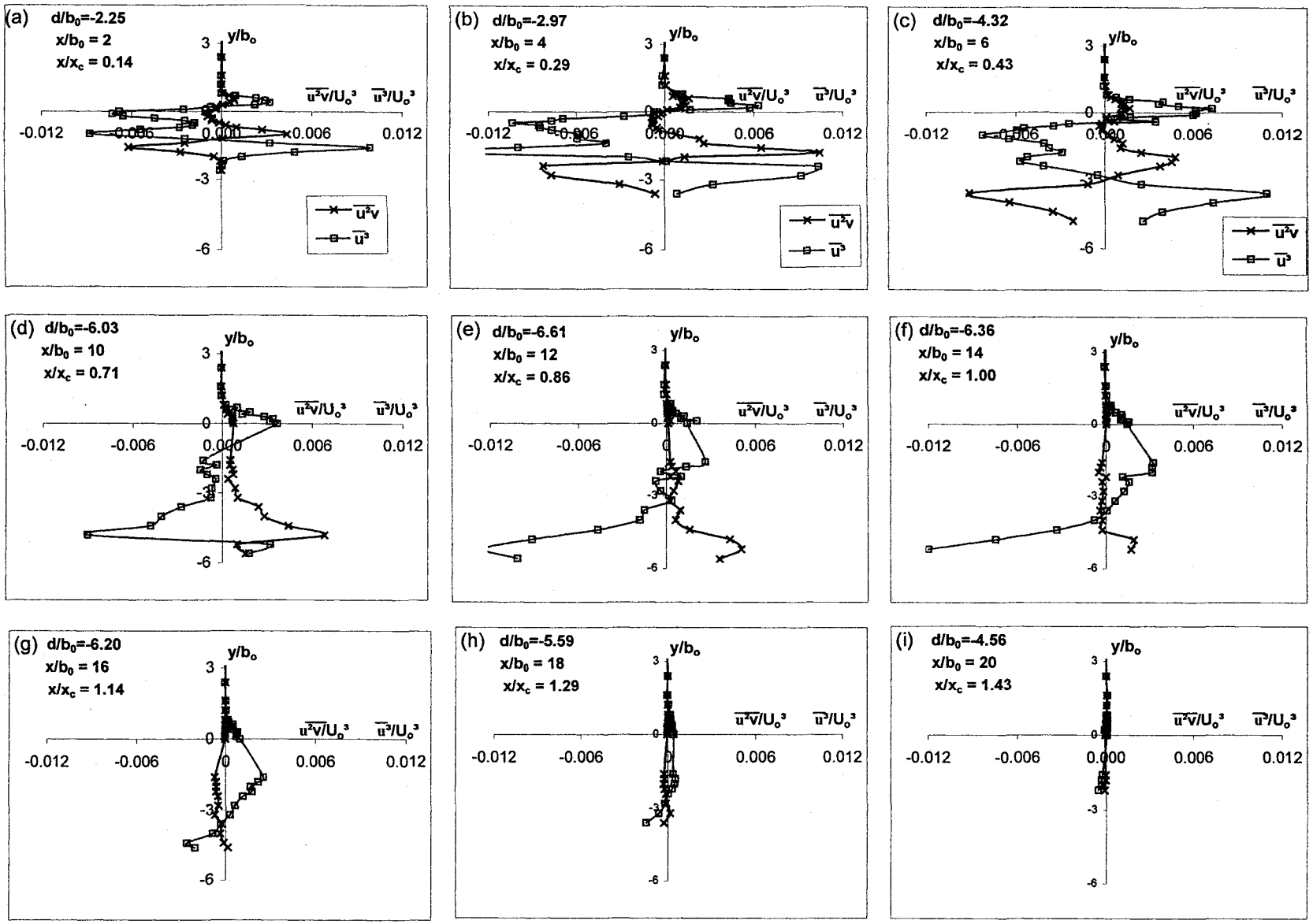

Figure 4.5.4: Turbulent diffusion in the direction normal to original bed and flux of the turbulent kinetic energy in the streamwise direction at various axial stations for Test A

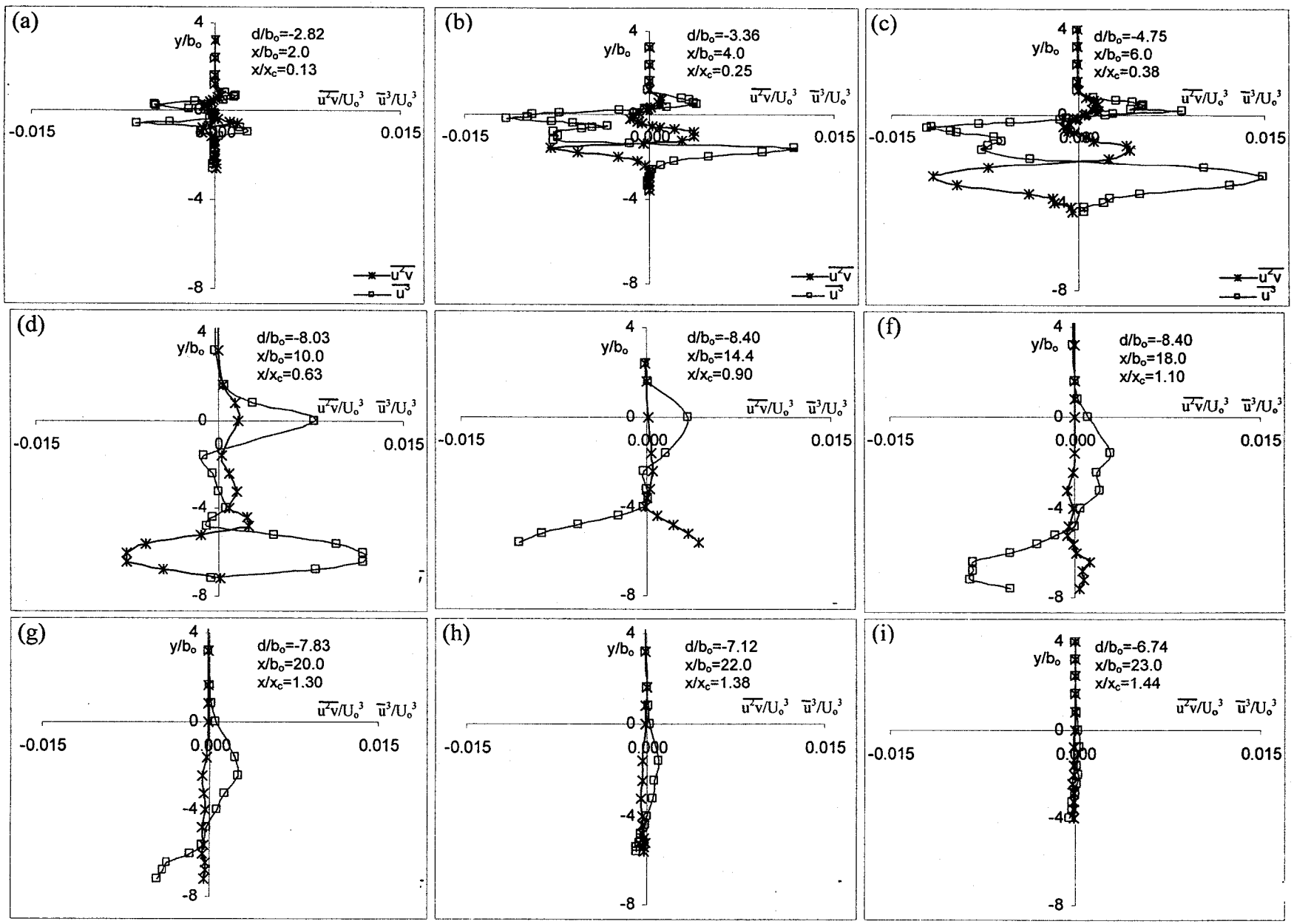

Figure 4.5.5: Turbulent diffusion in the direction normal to original bed and flux of the turbulent kinetic energy in the streamwise direction at various axial stations for Test B

sweeping motions could influence scour significantly. For the location farther up, absolute values of both D_v and $\overline{u^3}$ decrease and become zero at almost the same level (y/b_o = -1.2). This has significance as the changeover of sign indicates change in type of motion (ejection vs. sweep). Beyond this point, absolute values of both D_v and $\overline{u^3}$ increase and attain local peak values at y/b_o = -1.0, but once again with opposite sign. This time, D_v has a positive peak whereas $\overline{u^3}$ has a negative peak. Similar to the earlier peak values, the peak value of $\overline{u^3}$ is larger than the peak value of D_v. This indicates an upward transport of u momentum, whereas $\overline{u^3}$ is negative, indicating a slower moving fluid parcel. Together, $\overline{u^2v}$ and $\overline{u^3}$ indicate ejection of low speed fluid parcels that would be entrained into the jet.

With further increase of y/b_o, both variables approach zero. At y/b_o = -0.4 (which is also the location of maximum $\overline{U}$), $\overline{u^2v}$ attains a zero value. As y/b_o increases further ($\approx$ -0.1) both variables attain local peak values and both are negative. This indicates fluid particles enter the jet as entrainment from above the jet centreline. Just above the nozzle centreline (y/b_o = 0.4), $\overline{u^2v}$ and $\overline{u^3}$ both are positive, albeit slightly. This indicates that the fluid particle is being ejected and simultaneously moving a bit faster in the flow direction. Above this point, the value of both the variables reduces to almost zero and remains so for the rest of the depth. These have no direct influence on the effect of turbulence on scour.

Figures 4.5.4b and 4.5.5b for Tests A and Test B respectively show characteristics similar to those shown in Figure 4.5.4a (Test A) and Figure 4.5.5a (Test B). The magnitude of the peaks increase, which is indicative of higher level of turbulent activity. Figures 4.5.4c (Test A) and 4.5.5c (Test B) show characteristics similar to those shown in Figures 4.5.4a and 4.5.5a for Tests A and B respectively. Figure 4.5.4d for Test A and Figure 4.5.5d for Test B show both positive peak values (albeit very low) for $\overline{u^2v}$ and $\overline{u^3}$ near the sand bed [Figure 4.5.4d (y/b_o = -5.6,) and Figure 4.5.5d (y/b_o = -7.6,)]. This is an indication of the tendency for the fluid parcels to move in an upward direction. At this station, for y/b_o = -4.8 and for y/b_o = -7.0 for Test A and Test B respectively, both D_v and $\overline{u^3}$ attain peak values. D_v attains a positive peak whereas $\overline{u^3}$ attains a negative peak. Similar to the earlier peak values, the peak value of $\overline{u^3}$ is larger than the peak value of D_v. This indicates an upward transport of u momentum, whereas $\overline{u^3}$ is negative, indicating a slower fluid parcel motion. Together, $\overline{u^2v}$ and $\overline{u^3}$ indicate ejection of low speed fluid parcels that would be entrained into the jet. This type of motion can potentially contribute to suspending individual sand grains that can be transported by the mean flow. Farther from the bed and towards the free surface, the absolute value of both $\overline{u^2v}$ and $\overline{u^3}$ reduces and have no direct influence on the effect of turbulence on scour. Figures 4.5.4e to 4.5.4f and Figures 4.5.5e to 4.5.5f for Tests A and B respectively show characteristics similar to those shown in Figure 4.5.4d and Figure 4.5.5d and are all in the region of near-zero bed slope. Comparing Figure 4.5.4d with Figures 4.5.4e and 4.5.4f for Test A and Figure

4.5.5d with Figure 4.5.5e and Figure 4.5.5f for Test B, one can note that the magnitude of the peak for $\overline{u^3}$ increases and the magnitude of the peak for $\overline{u^2v}$ decreases with increasing distance from the nozzle and the jet-like characteristics diminish starting at Figure 4.5.4f and Figure 4.5.5f and beyond for Tests A and B respectively. Since one is close to the mean attachment point of the jet on the sand bed, the impingement causes large scale motion in all directions. This is reflected in the reduction of $\overline{u^2v}$ and $\overline{u^3}$ values. Figures 4.5.4h and 4.5.4i and Figures 4.5.5h and 4.5.5i for Test A and Test B respectively, show the profile in the positive slope region and indicate that the values for $\overline{u^2v}$ are close to zero throughout the depth of flow. This indicates very low turbulent diffusion in the y-direction. For this region, there is a reduction in the streamwise turbulent flux with increasing distance from the nozzle and eventually reaches zero, indicating a reduction in turbulent activities.

The ejection and sweeping type activities described above confirm the visual movement of sand grains noted earlier. At the location of two prominent fluid structures (at asymptotic conditions), there is very large negative $\overline{u^3}$ values with low turbulent diffusion. This may be one of the causes for sand particle movement at this location.

Figures 4.5.6 and 4.5.7 show variation of turbulent diffusion in the x direction $D_u = \overline{uv^2}$ and the variation of $\overline{v^3}$, which can be thought as the normal to the initial bed flux of the turbulent kinetic energy $\overline{v^2}$, at three axial stations for Test A and Test B respectively. Figures 4.5.6a, 4.5.6b and 4.5.6c show the variation in the region of negative bed slope, near-zero scour slope, and positive bed slope, respectively for Test A.

Similarly, Figures 4.5.7a, 4.5.7b and 4.5.7c show the variation in the region of negative bed slope, near-zero scour slope, and positive bed slope, respectively for Test B. From Figures 4.5.6a (Test A) and 4.5.7a (Test B), one can notice that there are several peak values in the profile. Peak values of the two variables occur at the same elevation. At this location, the sand bed is at a vertical distance of ~ $-3b_o$ and ~ $-5b_o$ from the nozzle axis for Test A and Test B respectively. Peak values near the bed ($y/b_o = -2.8$ for Test A and Test B) are indicative of sweeping type motion that can contribute to scour. The flow field confirms the description provided earlier. In the near-zero slope region (Figure 4.5.6b and Figure 4.5.7b) and close to the bed, $\overline{v^3}$ tends to be positive and $\overline{uv^2}$ is negative, which indicates ejection of slow moving fluid parcels. This can contribute to ejection of individual sand grains that can be transported by the mean flow. In the positive slope region (Figures 4.5.6c and 4.5.7c), both variables are negative at bed level. This indicates fluid particles enter the jet as entrainment from below the jet. Slightly above the bed, the value of both variables reduces to almost zero and remains so for the rest of the depth. Jet-like features are diminished at this location and turbulence has no direct influence on scour.

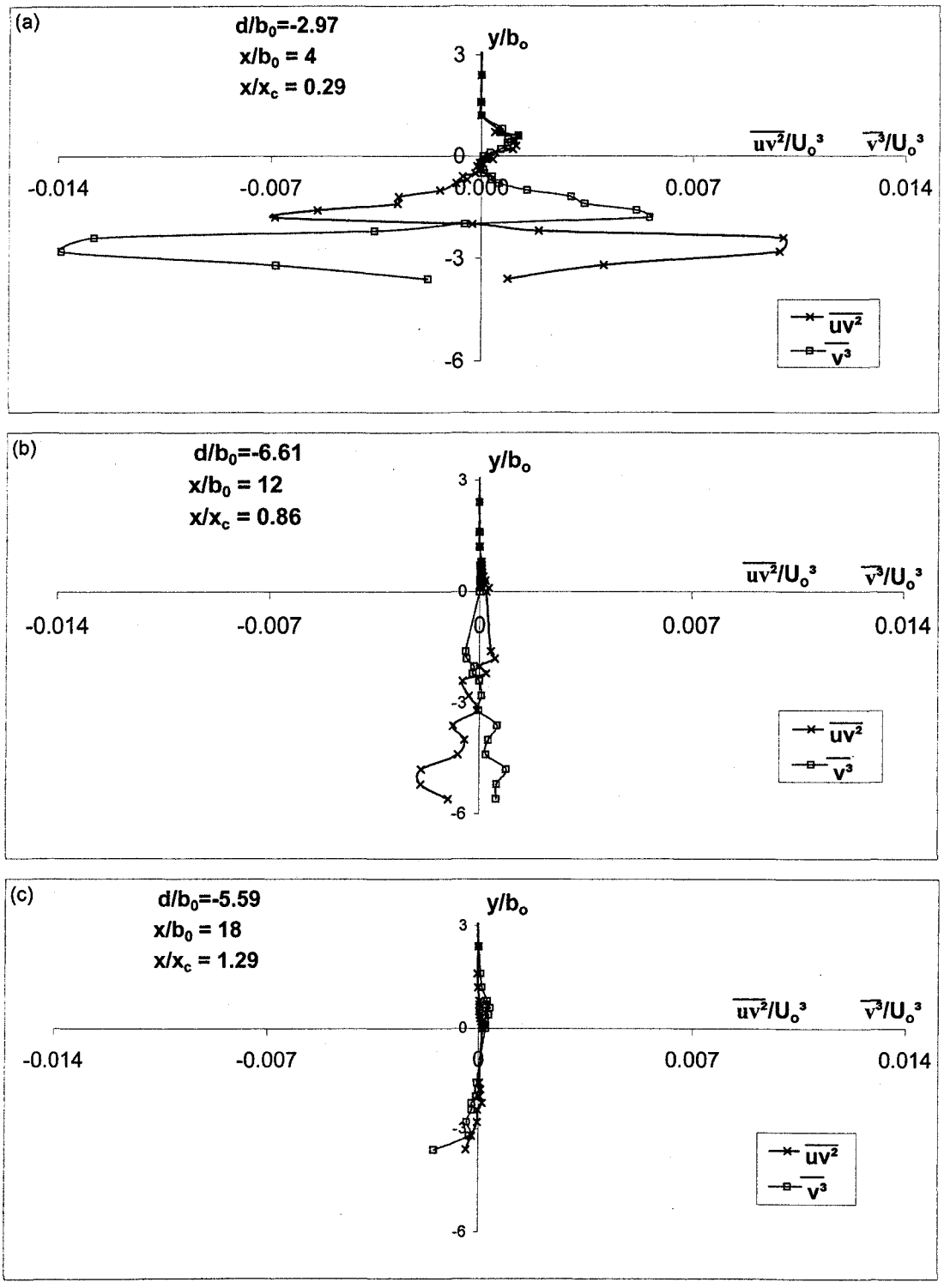

Figure 4.5.6: Turbulent diffusion in the streamwise direction and the flux of the kinetic energy in the direction normal to original bed at various axial stations for Test A

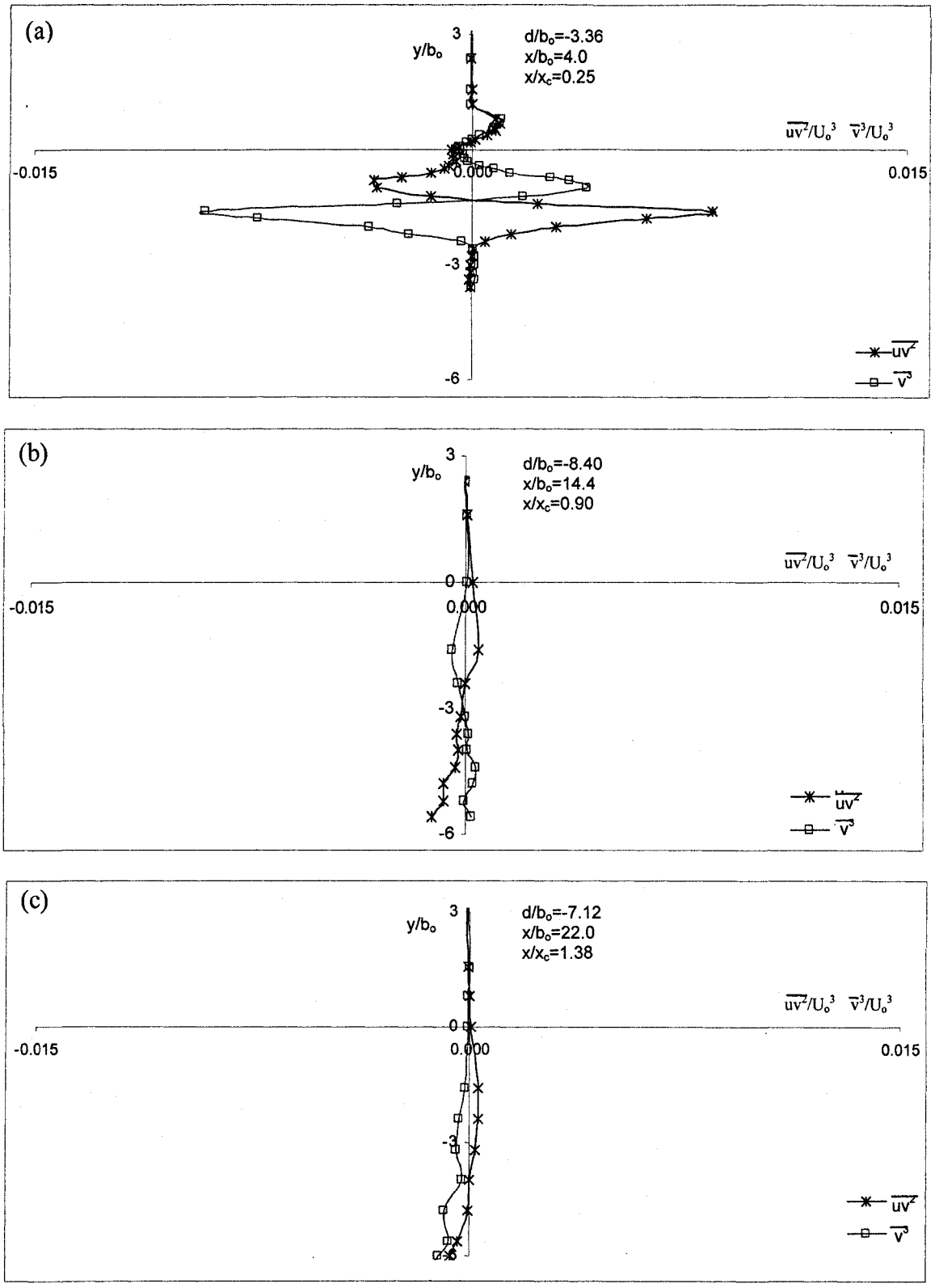

Figure 4.5.7: Turbulent diffusion in the streamwise direction and the flux of the kinetic energy in the direction normal to original bed at various axial stations for Test B

One can also view the combination of triple correlations as the average streamwise flux of total turbulent kinetic energy [KE $\approx$ $(0.5*(\overline{u^3}+\overline{uv^2}))$]. This is shown in Figures 4.5.8 and 4.5.9 for Test A and Test B respectively at various axial stations. Figure 4.5.8a shows the variation in the region of negative bed slope, Figure 4.5.8b shows the variation in the region of near-zero scour slope, whilst Figure 4.5.8c shows the variation in the region of positive bed slope for Test A. Similarly, Figure 4.5.9a shows the variation in the region of negative bed slope, Figure 4.5.9b shows the variation in the region of near-zero scour slope and Figure 4.5.9c shows the variation in the region of positive bed slope for Test B. From Figure 4.5.8a and Figure 4.5.4b for Test A and Figure 4.5.9a and Figure 4.5.5b for Test B, one can notice that the flux of KE is almost equal to turbulent diffusion $\overline{u^2v}$ for locations near the bed. Away from bed and near the nozzle centreline, the production of turbulent KE is much more than turbulent diffusion. The production term is high in this region as the jet is evolving through the turbulent zone. Both turbulent KE and turbulent diffusion reduce to zero at $y/b_o = 1.2$ for Tests A and B and remains so for the rest of the depth. From Figure 4.5.8b and Figure 4.5.4e (Test A) and Figure 4.5.9b and Figure 4.5.5e (Test B), one can notice that flux of turbulent KE is more than turbulent diffusion at the bed level. For this region of near-zero bed slope, the difference between flux of turbulent KE and turbulent diffusion increases with increase distance from the nozzle. Generation of turbulent energy in excess of dissipation influences scour in this region. The effect of this difference is apparent in the visible

vigorous sand particle movement in this region. For the region of positive bed slope, the values of streamwise flux of turbulent KE and turbulent diffusion are very close and reach zero values at locations close to the bed and remains the same for the depth of flow. For all axial stations, the value of flux of turbulent KE and turbulence diffusion is nearly zero from level $y/b_o = 1.2$ to the top of the flow for Test A and Test B.

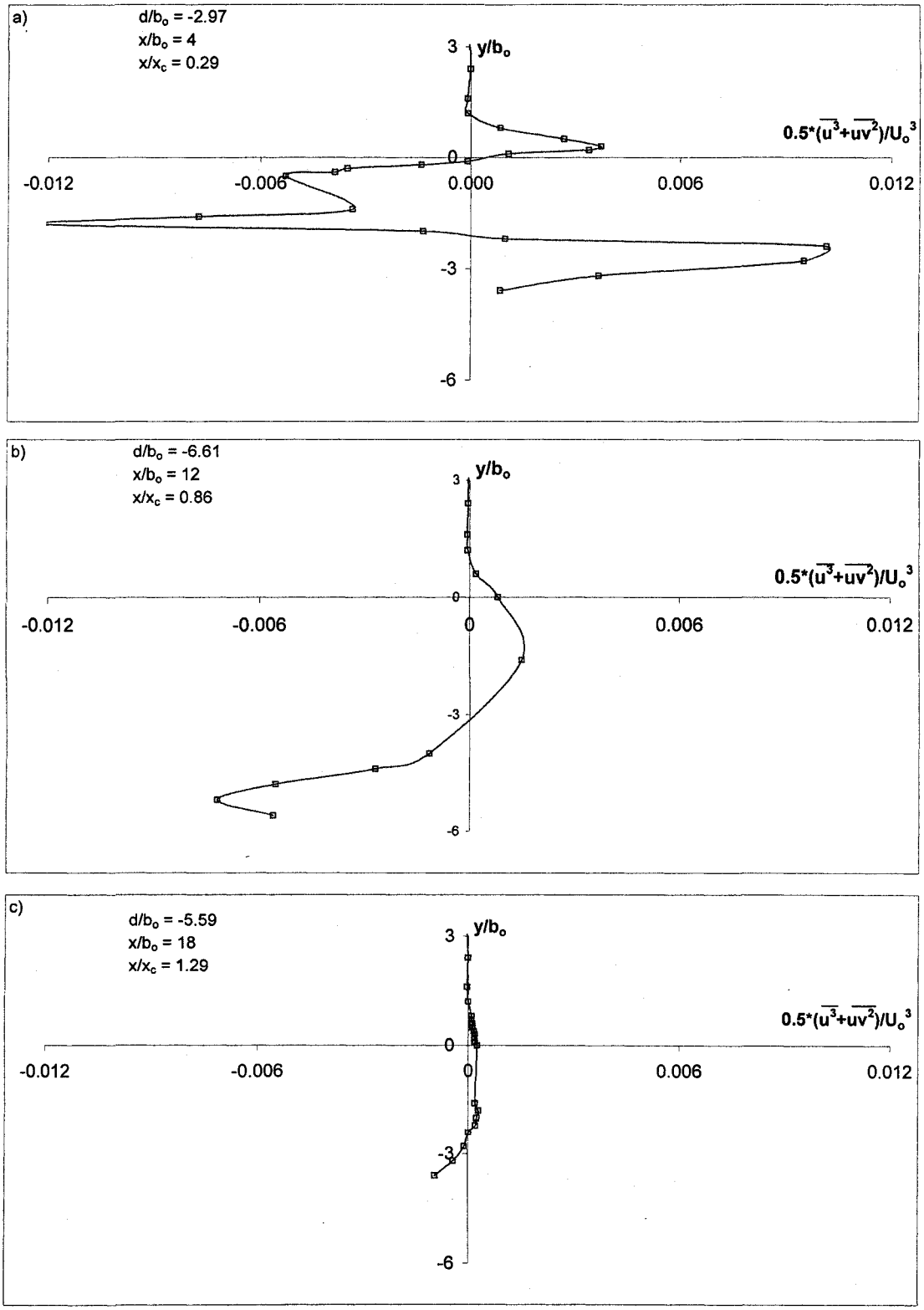

Figure 4.5.8: Average streamwise flux of total turbulent kinetic energy at various axial stations for Test A

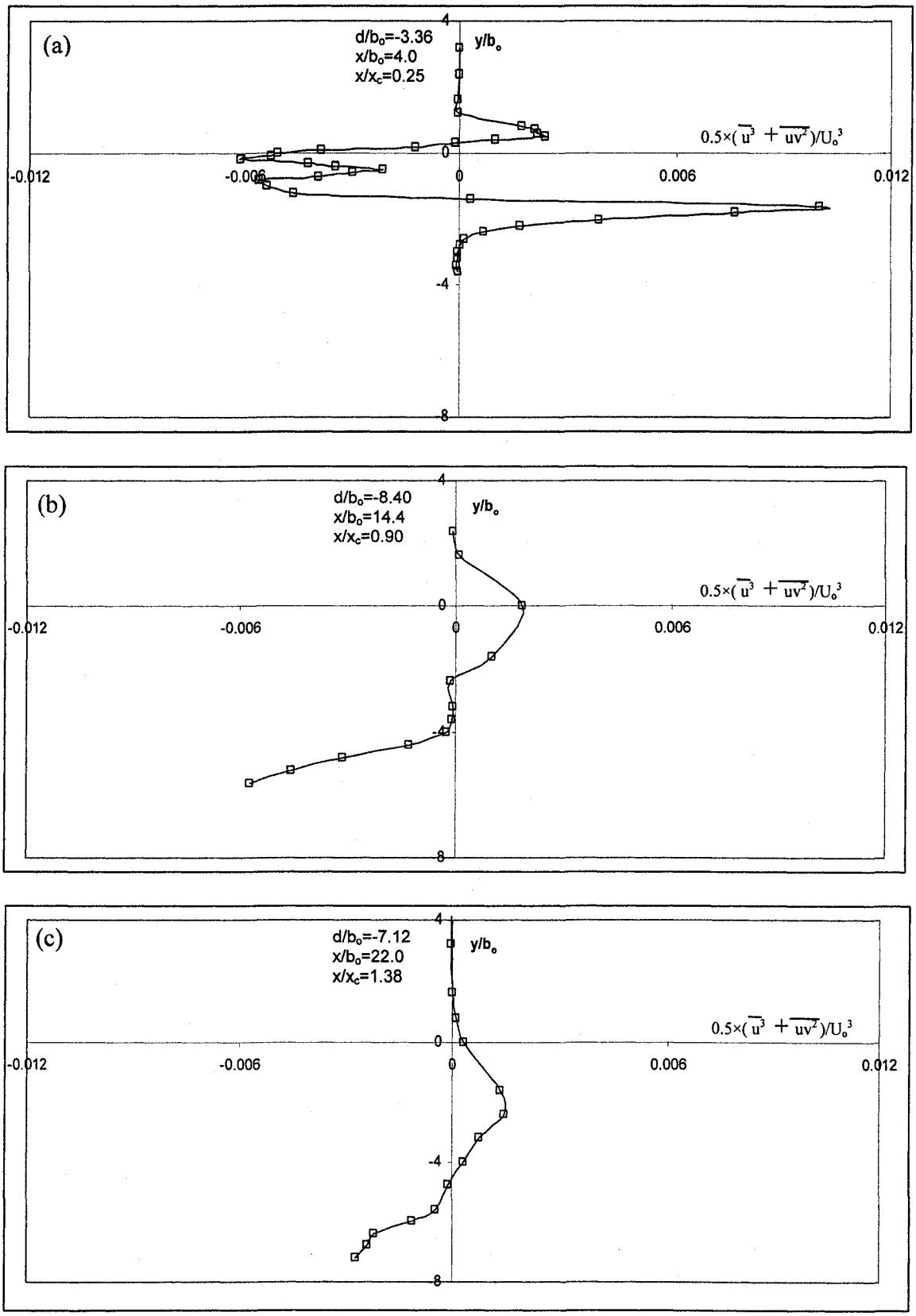

Figure 4.5.9: Average streamwise flux of total turbulent kinetic energy at various axial stations for Test B

4.6 Quadrant Analysis

In order to further understand the turbulent processes that take place at different locations in the flow, quadrant decomposition of the velocity fluctuations was carried out. Figure 4.6.1 shows the velocity data plotted in a u-v co-ordinate system at different near-bed locations. For each of the plots, threshold lines defined by $|uv| \geq H(u')(v')$ are used to denote extreme events. Here |uv| denotes the absolute of the instantaneous shear stress, u' and v' denotes the root-mean-square values of the fluctuations and H is a threshold value. This is done to separate background turbulence from large magnitude events that can potentially contribute to scour. Generally, data that lies below the threshold (H) is said to be in the hole and correspond to quieter periods. Data higher than threshold are indicative of stronger turbulent events and increasing values of H refer to much stronger events. Lines corresponding to H = 1, 2 and 3 are shown in the Figure 4.6.1. The procedure is very similar to that used in turbulent boundary layer analysis. For example, events in the domain with negative values of u and positive values of v (quadrant 2, Q2) would denote ejection of fluid parcels.

As one proceeds from the near-nozzle station in the negative bed slope region (Figures 4.6.1a to 4.6.1c), one can see a flurry of activity, and increase in quadrant 4 events, which corresponds to sweep events and can potentially cause scour. Even at a level of H = 3, the number of occurrence of extreme events is fairly large. It is important to recognize that Q2 events which represent ejections are reduced in progressing from Figure 4.6.1a to Figure 4.6.1c. Data in these figures are roughly distributed in the shape

of an ellipse with the major axis tilted and lying in Q2 and Q4. As one progresses to near-zero slope bed locations (Figures 4.6.1d to 4.6.1g), the major axis of the ellipse seems to gradually tilt towards the u axis. Moving from x/b_o = 10 (Figure 4.6.1d) towards the downstream to x/b_o = 16 (Figure 4.6.1g), one can note significant reduction in the sweeping motion and an increase of ejection at the threshold level H = 3. This is due to the contribution from the turbulent bursts noted earlier. On moving to the positive bed slope region (Figures 4.6.1h and 4.6.1i), data are very symmetrical and a lesser number of extreme events occur. From Figure 4.6.1 one can conclude that a significant portion of the near-bed turbulent events occur at the end of the negative bed slope region and the near-zero bed slope region, where one can notice more movement in sand grains.

Figures 4.6.2 and 4.6.3 show the contribution to the mean shear stress by the extreme events at a threshold level H = 2 at various axial stations for Test A and Test B respectively. Both plots are qualitatively similar. Only those data points that lies outside the hole region are used to calculate the mean. In the negative slope region both Q2 (ejection) and Q4 (sweep) events are important with sweep events lying closer to the bed. In the near-zero bed slope region, Q4 events are reduced but ejection events can cause individual grains to be suspended into the flow and to be transported downstream. For positive slope the extreme events reduce in number. Outward (Q1) and inward interaction (Q3) are significant within the core of the jet up to a distance $6b_o$ from the nozzle and are not important farther from the nozzle as the jet gets fairly diffused.

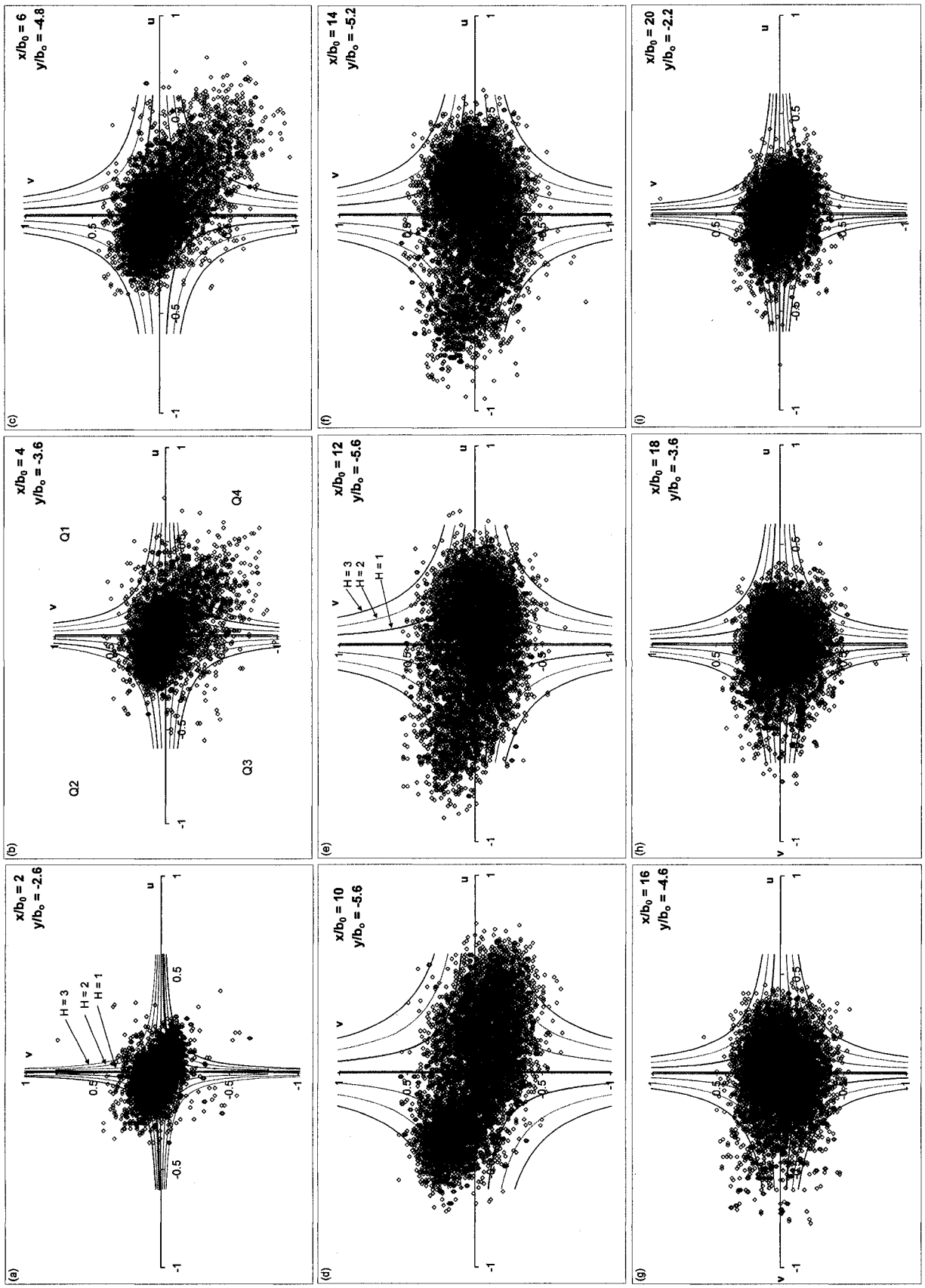

Figure 4.6.1: Plot of velocity fluctuations in u-v co-ordinates at various near-bed locations

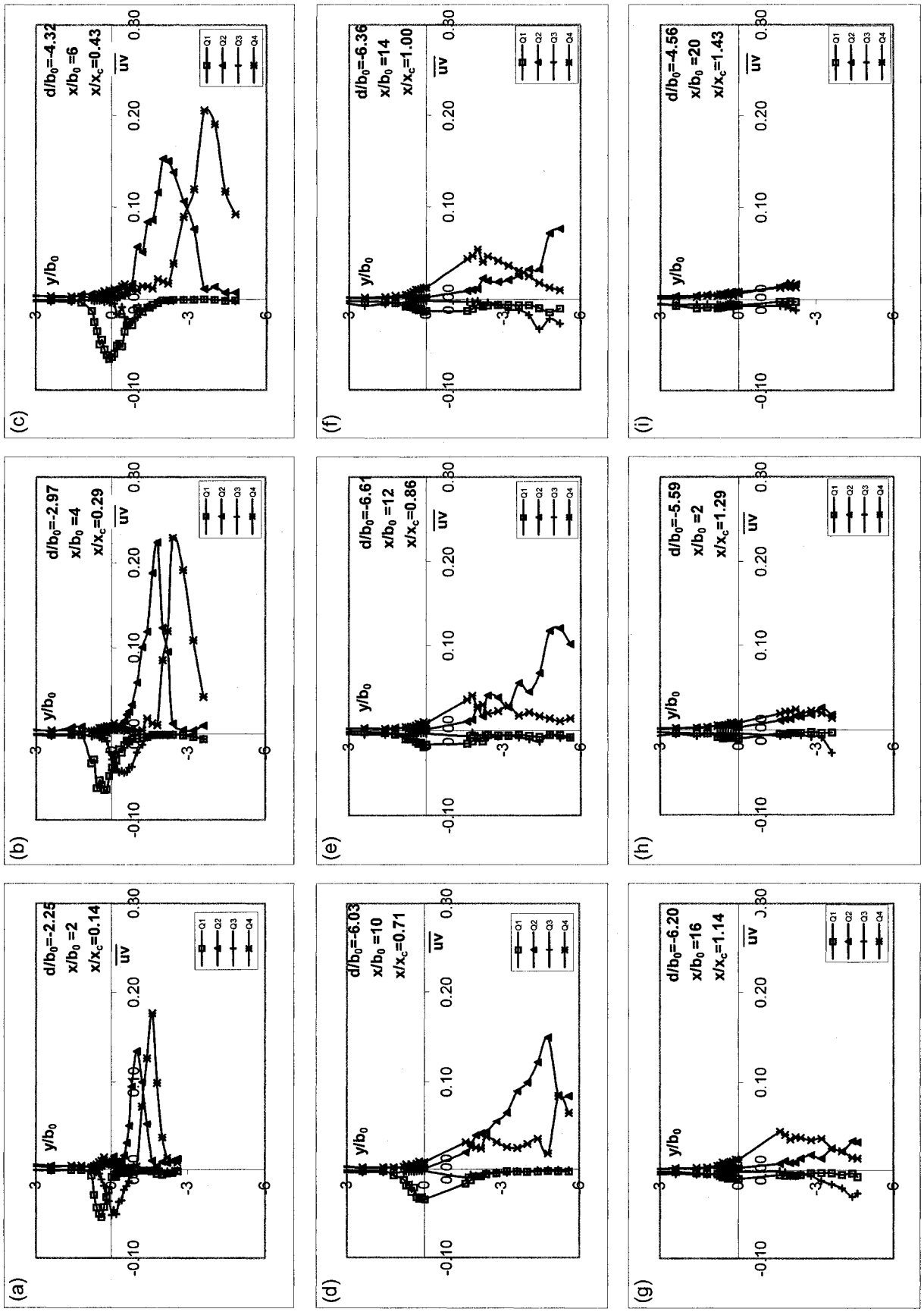

Figure 4.6.2: Shear stress contribution by extreme events for H = 2 at various axial stations for Test A

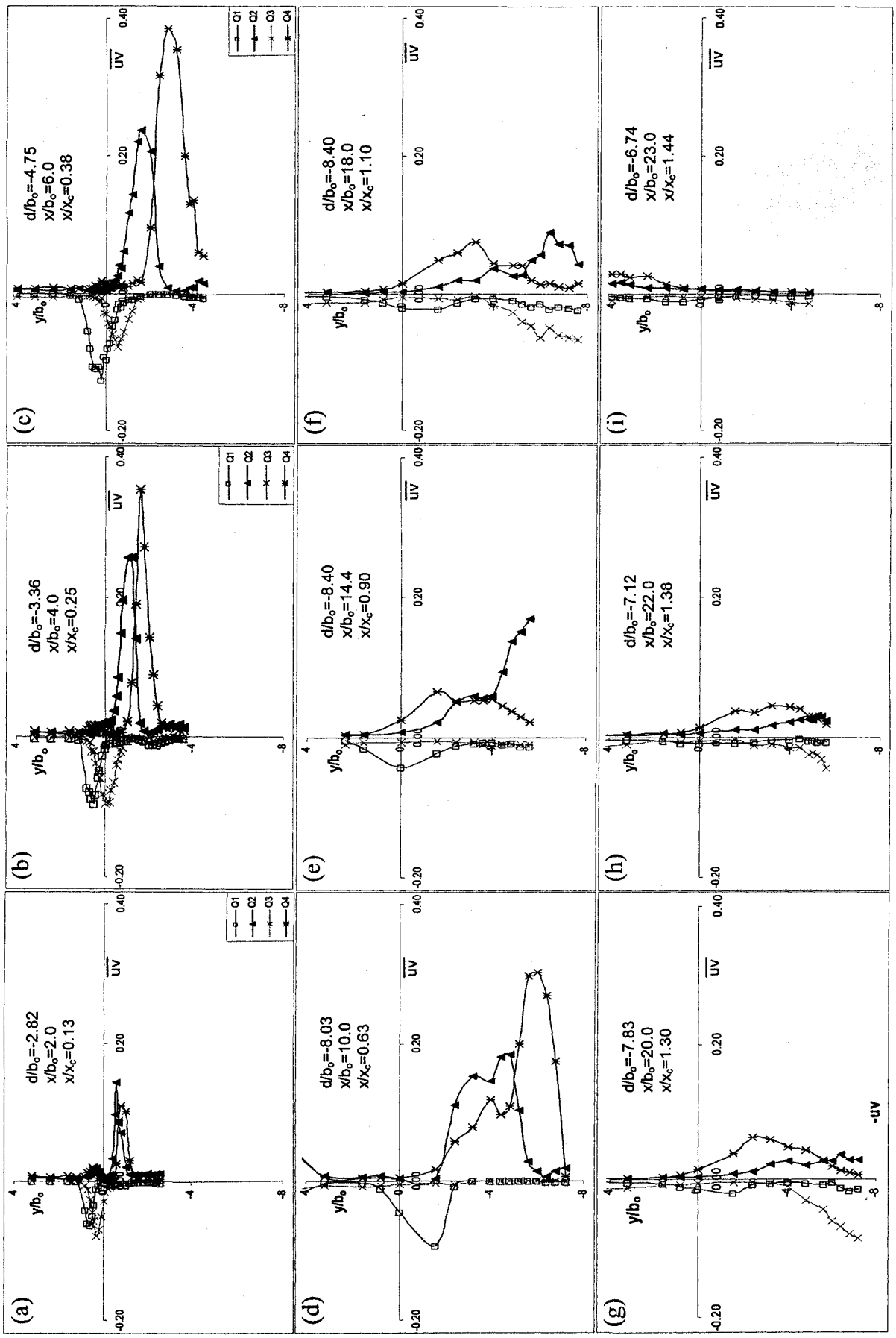

Figure 4.6.3: Shear stress contribution by extreme events for H = 2 at various axial stations for Test B

4.7 Presence of Vortex in 'Scoop and Throw' Regime

As indicated in the visual observation section, two counter-rotating vortices were seen to occur in the scour region (for the time period 3 hrs $\leq t \leq$ 72 hrs). The vortices were active in the 'scoop and throw' region as shown in Figure 4.2.1 (C-D and E-F regions). The presences of the vortices were confirmed by dye visualization and movement of sand particles in the scour hole. Figures 4.7.1a to 4.7.1d shows the v component histogram in the region of interest at various elevations. Negative v will indicate downward directed motion. Since the laboratory is equipped only with a two-dimensional LDA system, the third velocity component (w) could not be directly obtained. Additional measurements were made by placing the LDA probe at an angle (see Figure 4.7.1e insert) with the streamwise direction to obtain an estimate of velocity in the z direction. Figures 4.7.1e to 4.7.1h show the velocity histogram obtained in the plane of measurement. Negative value of this histogram indicates motion towards the near side wall and positive value of the same indicates motion towards the far side wall. As indicated in the histograms, the number of negative measurements decreased as one moves upwards from the near-bed location. These measurements are only qualitative and used to evaluate the fluid motion towards the wall. Together with the vertical measurement (Figures 4.7.1a to 4.7.1d), one can clearly see a rotational motion that is directed towards the inner side wall in the bottom regions and away from the inner side wall for the upper locations and serves to confirm the presence of a vortex structure.

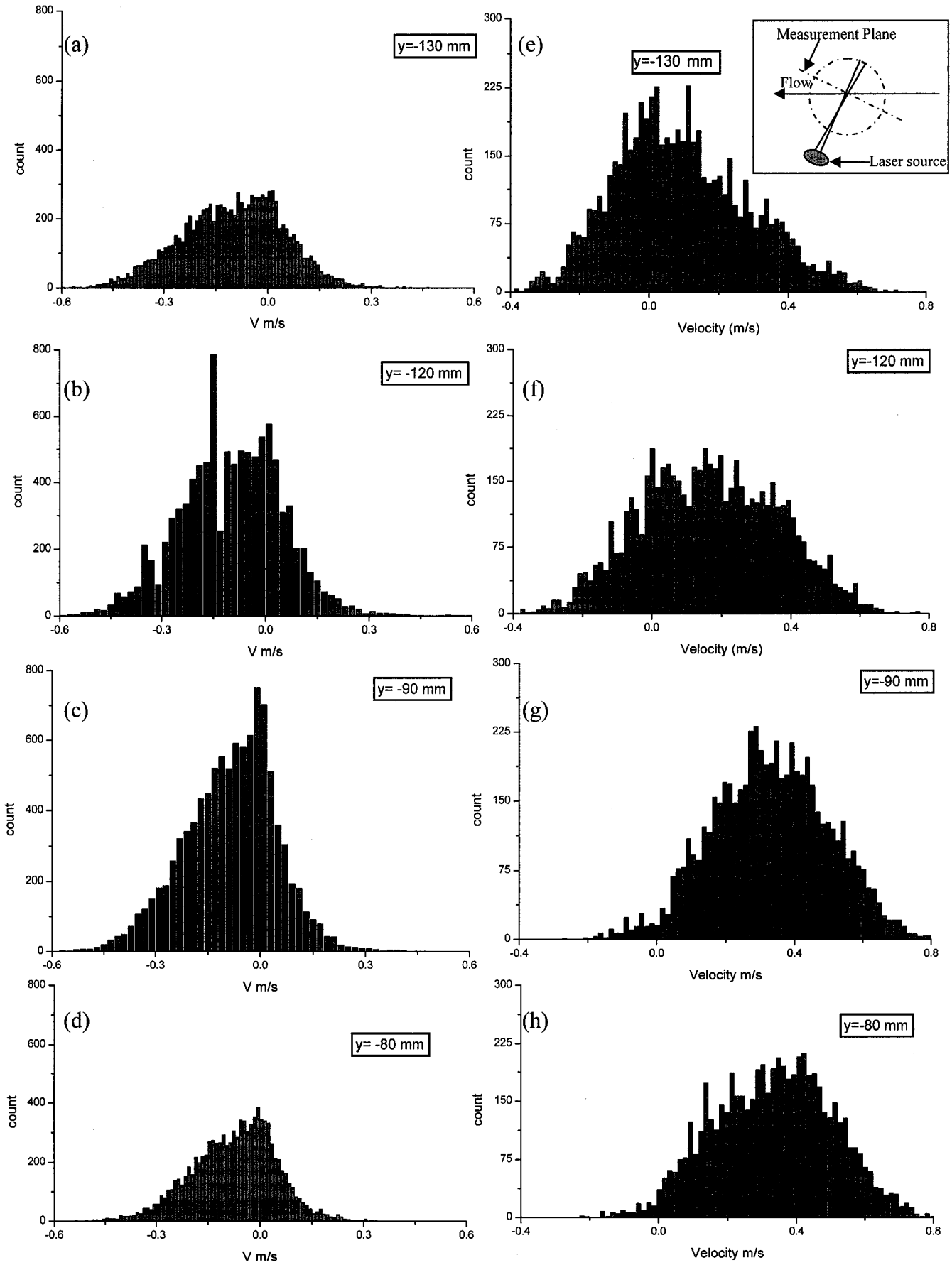

Figure 4.7.1: v-histogram and estimate of w-histogram at $x/b_o = 14$

CHAPTER 5

CONCLUSIONS AND RECOMMENDATIONS FOR FUTURE WORK

5.1 Conclusions

An experimental study was carried out to further understand the role of fluid structures in causing scour. The present study indicates the presence of different types of flow structures during various time periods. Both visual observation and velocity measurements aided in deciphering the role of fluid structures. Even for regions near the nozzle, the present jet did not demonstrate free jet characteristics. This is to be expected due to bed confinement on one side and the large scale recirculation zone situated above the jet on the other side. The growth rate of the jet is larger towards the bed due to the excess turbulence created by the water-sediment interaction. Furthermore, the vertical component of the mean velocity above the jet centreline is different from that of a free jet. This is a consequence of the influence of the recirculating zone above the jet.

At the beginning, the scour was vigorous and accompanied by large scale suspension of sand grains. This is similar to the observations by several researchers. With progress of time (600 s $\leq$ t $\leq$ 3 hrs) two or three longitudinal streaks and very prominent concave depressions were observed. These longitudinal streaks and concave depression form and disappeared rapidly in the scour hole region. The streaks are very similar to that noticed by Hopfinger et al. (2004). However, Hopfinger et al. (2004) did not report the presence of the concave shaped depressions. The formation and disappearance of the streaks continued for a relatively significant period. Hopfinger et al. (2004) observed loose sediment streaks or longitudinal ridges on the positive bed slope in the scour hole

but for the present tests streaks were observed mostly in the near-zero bed slope and at the beginning of positive bed slope.

After sufficient progress of the scour, a 'scoop and throw' scouring action replaced streak-like features (3 hrs $\leq t \leq$ 24 hrs). The 'scoop and throw' occurs in the vicinity of the streak-like features. A lifting spiraling motion of sand particles was observed during this period indicating some vortex activity. For the period 24 hrs $\leq t \leq$ 72 hrs, scour hole progress continued at a slower pace with slower 'scoop and throw' scouring action. Small scale bed suspension could be noticed during this time period.

Frequent and random turbulent bursts were observed in the near-bed region across the cross-section of the flume when the scour hole attains a near asymptotic state ($t >$ 72 hrs). These bursts caused the movement of sand particles close to the bed region. Two prominent scour mechanisms were also observed occurring on either side of the flume axis. Sand particles appeared to be spiraled towards the side walls and the flume axis due to this motion. It should be remarked that at asymptotic conditions, the back and forth movement of the impingement point, the frequent but random turbulent bursts and the two prominent scour mechanisms, all occurred at one time or the other. The jet impingement tends to cause a limited suspension and lifting of the sand particles into the flow stream where they are picked up and transported by the higher velocity fluid parcels. In addition, the fluid structures caused vigorous lateral movement. It is however noteworthy that in spite of these actions, any changes in the instantaneous bed profile was a local phenomenon and did not cause significant change in the overall mean bed profile.

There was also no large scale movement of bed particles anywhere within the flow field at asymptotic conditions.

At the asymptotic state, the scour profile in the hole region was nominally two-dimensional across the width of the flume. However, in the mound region, the lateral profile was not two-dimensional and has two distinct peaks. These peaks occur closer to the side walls leaving a trough in the centre portion of the mound.

The jet impingement point moved back and forth and the mean location of impingement was close to the maximum scour depth. The wide range of variation in instantaneous velocity from positive to negative values is a clear indication of back and forth movement of jet.

Most of the turbulent activity occurred at the end of the negative slope region and continued till the start of the positive bed slope region. Analysis of the triple correlations and quadrant decomposition indicates sweep type events in the region which can contribute to scour. Ejection type activity also occurred which suspends sand particles that can be carried away by the mean flow. Though the velocity measurements were conducted at asymptotic conditions, one can extrapolate to other time periods and conclude that the sweep and ejection contribute significantly to the scour process.

The motion of the impingement point, occurrence of two prominent fluid structures and turbulent bursts cause vigorous sand particle movement in the near-zero bed slope region. Presence of very high streamwise turbulent flux and almost zero turbulent diffusion in this zone validate the above-mentioned activity. The present

comprehensive velocity data set will be of assistance in validating future numerical models.

5.2 Recommendations for Future Work

On the basis of the above conclusions and our current attempt at qualitatively explaining the scour process by a plane wall jet, the following recommendations are relevant for future work:

1. Study the role of fluid structures as a function of channel width.
2. Study the role of fluid structures when aprons are introduced at the jet exit.

References

Aderibigbe, O. and Rajaratnam, N. (1998). "Effect of sediment gradation on erosion by plane turbulent wall jets." *ASCE Journal of Hydraulic Engineering*, 124(10), 1034-1042.

Ali, K.H.M. and Lim, S.Y. (1986). "Local scour caused by submerged wall jets." *Proceedings of Institution of Civil Engineers*, Part 2, 81, 607-645.

Ali, K.H.M. and Neyshaboury, S.A.A. (1991). "Localized scour downstream of a deeply submerged horizontal jet." *Proceedings of the Institution of Civil Engineers*, Part 2, 91, 1-18

Annandale, G.W. (2004). Keynote Address, Second International Conference on Scour and Erosion, Singapore.

Balachandar, R. and Kells, J.A. (1997). "Local channel scour in uniformly graded sediments: the time-scale problem." *Canadian Journal of Civil Engineering*, 24(5), 799-807.

Balachandar, R., Kells, J.A. and Thiessen, R.J. (2000). "The effect of tailwater depth on the dynamics of local scour." *Canadian Journal of Civil Engineering*, 27(1), 138-150.

Belatos, S. and Rajaratnam, N. (1977). "Impingement of axisymmetric developing jets." *Journal of Hydraulic Research*, 15(4), 311-326.

Breusers, H.N.C. and Raudkivi, A.J. (1991). *Scouring.* Hydraulic Structures Design Manual 2, International Association for Hydraulic Research, A.A. Balkema, Rotterdam, The Netherlands.

Chatterjee, S.S. Ghosh, S.N. and Chatterjee, M. (1994). "Local scour due to submerged horizontal jet." *ASCE Journal of Hydraulic Engineering*, 120(8), 973-993.

Deshpande, N.P. (2004). "Effects of submergence and test startup conditions on local scour by plane turbulent wall jets." M.A.Sc. Thesis, University of Windsor, Ontario, Canada.

Dey, S. and Barbhuiya, A.K. (2004). "Clear water scour at abutments." *Water Management Journal, Proceedings of the Institute of Civil Engineers,* 157(2), 77-97.

Faruque, M. A. A. (2004). "Transient local scour by submerged three dimensional wall jets: Effect of tailwater depth." M.A.Sc. Thesis, University of Windsor, Ontario, Canada.

Hogg, A. J., Huppert, H.E. and Dade, W.B. (1997). "Erosion by planar turbulent wall jets." *Journal of Fluid Mech.,* 338, 317-340.

Hopfinger, E.J., Kurniawan, A., Graf, W.H. and Lemmin, U. (2004). "Sediment erosion by Görtler vortices: the scour-hole problem." *Journal of Fluid Mech.,* 520, 327-342.

Johnston, A.J. (1990). "Scourhole developments in shallow tailwater." *Journal of Hydraulic Research*, 28(3), 341-354.

Karim, O.A. and Ali, K.H.M. (2001). "Prediction of flow patterns in local scour holes caused by turbulent water jets." *Journal of Hydraulic Research,* 38(4), 279-287.

Karlsson, R.I., Eriksson, J. and Persson, J. (1992). "LDV measurements in a plane wall jet in a large enclosure." *6th International Symposium on Applications of Laser Techniques to Fluid Mechanics,* 1.5.1-1.5.6

Kells, J.A., Balachandar, R. and Hagel, K.P. (2001). "Effect of grain size on local channel scour below a sluice gate." *Canadian Journal of Civil Engineering,* 28(3), 440-451.

Kline, S.J. and McClintock, F.A. (1953). "Describing uncertainties in single-sample experiments." *Mechanical Engineering*, 75, 3-8.

Kouchakzadeh, S. and Townsend, R.D. (1997). "Maximum scour depth at bridge abutments terminating in the floodplain zone." *Canadian Journal of Civil Engineering,* 24(6), 996–1006.

Laursen, E.M. (1952). "Observations on the nature of scour." *Proceedings of the 5th Hydraulic Conference*, Bulletin 34, State University of Iowa, 179-197.

Mason, P.J. and Arumugam, K. (1985). "Free jet scour below dams and flip buckets." *ASCE Journal of Hydraulic Engineering,* 111(2), 220–235.

Moffat, R.J. (1988). "Describing the uncertainties in experimental results," Experimental Thermal and Fluid Science, 1, 3-17.

Mohamed, M.S. and McCorquodale, J.A. (1992). "Short-term local scour." *Journal of Hydraulic Research*, 30(5), 685-699.

Neyshabouri, S.A.A., Barron, R. and Ferreira da Silva, A.M. (2001). "Numerical simulation of scour by a wall jet." *Water Engineering Research*, 2(3), 179-185.

Quinn, W. R. and Militzer, J. (1988). "Experimental and numerical study of a turbulent free square jet." *Journal of Physics of Fluids*, 31(5), 1017-1025.

Rajaratnam, N. (1981). "Erosion by plane turbulent jets." *Journal of Hydraulic Research*, 19(4), 339-358.

Rajaratnam, N., Aderibigbe, O. and Pochylko, D. (1995). "Erosion of sand beds by oblique plane water jets." *Proceedings of the Institution of Civil Engineers, Water Maritime and Energy*, 112(1), 31-38.

Rajaratnam, N. and Berry, B. (1977). "Erosion by circular turbulent wall jets." *Journal of Hydraulic Research*, 15(3), 277-289.

Rajaratnam, N. and Humphries, J.A. (1984). "Turbulent non-buoyant surface jets." *Journal of Hydraulic Research*, 22(2), 103-115.

Rajaratnam, N. and Macdougall, R.K. (1983). "Erosion by plane wall jets with minimum tailwater." *Journal of Hydraulic Engineering*, ASCE, 109(7), 1061-1064.

Sarathi, P. (2005). "Scour by submerged square wall jets at low densimetric Froude numbers." M.A.Sc. Thesis, University of Windsor, Ontario, Canada.

Schwarz, A.C., Plesniak, M.W. and Murthy, S.N.B. (1999). "Turbulent boundary layers subjected to multiple strains." *Transactions ASME Journal of Fluids Engineering*. 121, 526-632.

Tachie, M.F. (2000). "Open channel turbulent boundary layers and wall jets on rough surfaces." Ph. D. Thesis, University of Saskatchewan, Saskatchewan, Canada.

Tarapore, Z.S. (1956). "Scour below a submerged sluice gate." M.Sc. Thesis, University of Minnesota, Minnesota, USA.

Topping, J. (1957). *Errors of Observation and Their Treatment*. The Institute of Physics, London, 119p.

Ushijima, A. (1996). "Arbitrary Lagrangian-Eulerian numerical prediction for local scour caused by turbulent flows." *Journal of Computational physics*, 125, 71-72.

Wu, S. and Rajaratnam, N. (1995). "Free jumps, submerged jumps and wall jets." *Journal of Hydraulic Research*, 33(2), 197-212.

Yanta, W.J. and Smith, R.A. (1973). *AIAA 11th Aerospace Sciences Meeting*, Washington DC, Paper 73-169.

APPENDIX A

SOIL GRADATION

The sand bed gradation measurements are shown in Table A.1. The characteristics indicate that the sand can be said to be reasonably uniform and well-graded. Breusers and Raudkivi (1991) mention that when the ratio $d_{95}/d_5 < 5$ and the geometric standard deviation σ_g is < 1.35, the sand can be described as uniform. The coefficient of curvature, C_z, is a measure of the gradation of the sand. The values of C_z between 1 and 3 indicate well-graded sand. (Aderibigbe and Rajaratnam, 1998).

Gradation measurements	
d_{50} (mm)	2.15
d_{95}/d_5	1.87
σ_g	1.28
C_z	1.14

Table A.1: Gradation measurements of the sand bed

APPENDIX B

DATA

The data for all the figures plotted in this thesis can be found on the enclosed CD-ROM.

APPENDIX C

UNCERTAINTY ANALYSIS

The uncertainty analysis presented below is based on the methodology outlined in Kline and McClintock (1953) and Moffat (1988). A 95% confidence interval is assumed in the following analysis. The main source of error in the LDA measurements is the uncertainty in the determination of the frequency present in each burst by the processor. In addition to the above, the uncertainty in statistical quantities will also depend on the sample size (N).

A methodology for estimating uncertainty in LDA measurements was developed by Yanta and Smith (1973) and Schwarz et al. (1999). They derived the following relations for the uncertainty in the streamwise and vertical components of the mean velocity respectively:

$$\frac{\sigma_U}{\overline{U}} = \left[(\sigma_o)^2 + \frac{1}{N}\left(\frac{u}{U}\right)^2 \right]^{1/2} \qquad \text{Eq.1}$$

$$\frac{\sigma_V}{\overline{V}} = \left[(\sigma_o)^2 + \frac{1}{N}\left(\frac{v}{V}\right)^2 \right]^{1/2} \qquad \text{Eq. 2}$$

where σ_o is the error due to the uncertainty in the determination of the beam-crossing angle and N is the number of samples.

The corresponding expressions for the streamwise and vertical components of the turbulence fluctuations and the Reynolds shear stress are respectively given by:

$$\frac{\sigma_u}{u} = \left[(\sigma_o)^2 \left(\frac{\langle uv \rangle}{u^2} \right) + \frac{1}{2N} \right]^{1/2} \qquad \text{Eq. 3}$$

$$\frac{\sigma_v}{v} = \left[(\sigma_o)^2 \left(\frac{\langle uv \rangle}{v^2} \right) + \frac{1}{2N} \right]^{1/2} \qquad \text{Eq. 4}$$

$$\frac{\sigma_{\langle uv \rangle}}{\langle uv \rangle} = \left[(\sigma_o)^2 \left(1 + \frac{u^2}{\langle uv \rangle} \right)^2 + \frac{1}{N} \left(\frac{2}{R} \right) \right]^{1/2} \qquad \text{Eq. 5}$$

R is the shear stress correlation coefficient .

Following Schwarz et al. (1999) a value of $\sigma_o = 0.4$ is adopted in the present analysis. Typical estimates of uncertainties for the mean and fluctuating quantities are given in Table C.1 using the test conditions for Test A.

$\bar{U}$ (%)	$\bar{V}$ (%)	u (%)	v (%)	<uv> (%)
0.4	0.4	0.6	0.5	2.5

Table C.1: Typical uncertainty estimates for Test A

Following methods based on Topping (1957), the uncertainty for other quantities can be estimated from the following expression:

$$P_r = \left[\sum_{k=1}^{M} (P_J)^2{}_k\right]^{\frac{1}{2}} \qquad \text{Eq. 6}$$

J is the number of variables, M is the number of sources of repeatability error and P_J is twice the standard deviation of the variable J.

The bias in the measurement of a variable was estimated by the following expression:

$$B_r = \left[\sum_{k=1}^{M} (B_J)^2{}_k\right]^{\frac{1}{2}} \qquad \text{Eq. 7}$$

where J and M are as defined in Eq. 6. B_J is the measure of the bias error from a source. The total error estimate, U_r, is obtained by the expression:

$$U_r = \left(B_r{}^2 + P_r{}^2\right)^{\frac{1}{2}} \qquad \text{Eq. 8}$$

From the above expressions, using a digital caliper with 0.01 mm precision to measure the nozzle opening yielded an error estimate of 4%. Similarly, using a graduated measuring rule with 1 mm precision to measure the tailwater depth (y_t) yielded an error estimate of 1%. Using similar methods, the error estimates for other measured and derived quantities at 95% confidence level are summarized in Table C.2.

Quantity	Error (%)
b_o	4.00
d_{50}	3.00
F_o	4.76
F_r	1.13
y_t	0.99
y_t/b_o	1.03

Table C.2: Error estimates in measured and derived quantities

VITA AUCTORIS

Alex Bey was born in 1968 in Agate, Ghana. He graduated from the Presbyterian Boys Secondary School, Legon in 1988. From there he went on to the University of Science and Technology where he obtained a B.Sc. in Civil Engineering in 1993. He is currently a candidate for the Master's degree in Civil Engineering at the University of Windsor and hopes to graduate in Summer 2005.